SEISMIC FRAGILITY ANALYSIS OF BRIDGE ABUTMENTS

A DISSERTATION

Submitted in the partial fulfilment of the requirements for the award of the degree of

MASTER OF TECHNOLOGY

in

EARTHQUAKE ENGINEERING

(With specialization in Structural Dynamics)

by

AMAN SRIVASTAVA

(17526003)

DEPARTMENT OF EARTHQUAKE ENGINEERING
INDIAN INSTITUTE OF TECHNOLOGY ROORKEE
ROORKEE-247 667 (INDIA)

JUNE, 2019

CANDIDATE'S DECLARATION

I hereby, declare that the work which is being presented in this dissertation report entitled, **"SEISMIC FRAGILITY ANALYSIS OF BRIDGE ABUTMENTS"**, being submitted in partial fulfilment of the requirements for the award of degree of "Master of Technology" in "Earthquake Engineering" with specialization in Structural Dynamics, to the Department of Earthquake Engineering, Indian Institute of Technology Roorkee, under the supervision of Prof. Yogendra Singh, Department of Earthquake Engineering, Indian Institute of Technology Roorkee, is an authentic record of my own work carried out during the period of June 2018 to June 2019.

Place: Roorkee **Aman Srivastava**

Date: Enrollment no. 17526003

CERTIFICATE

This is to certify that the above statement made by the candidate is correct to the best of my knowledge and belief.

Place: Roorkee **(Yogendra Singh)**

Date: Professor

Department of Earthquake Engineering

Indian Institute of Technology Roorkee

ABSTRACT

Bridges have always been one of the most vulnerable structures during a seismic event. Design philosophy of bridges being completely different from that of buildings, these are faced with completely different challenges. One of the major bridge component susceptible to damage during a seismic event is abutment. Its performance is affected due to ignoring of some crucial factors, ultimately resulting in failure of the whole bridge, as has been seen in the past earthquakes. The main drawback in the present design of bridge abutment is the ignoring of the soil-structure-interaction between the abutment and the retained backfill. In the past, many researches have contributed to the development of a design philosophy of abutments by simulating the static and seismic earth pressure distribution. The principle aim of the present study is to extend this method to a coupled abutment-backfill system. In this dissertation, finite element (FE) models have been developed to study seismic response and vulnerability of abutments through development of fragility curves.

To start with, a classic earth pressure problem of a vertical wall retaining a horizontal backfill is considered to understand the behavior of the system. A 2D finite element analysis is performed using ABAQUS with rigid wall retaining frictional soil. Backfill soil is modelled using plane-strain quadratic quadrilateral (CPE8R) elements using Mohr-Coulomb failure criteria. Pseudo-static methodology is used to account for the horizontal inertial component of the system during a seismic event. Further, the key parameters effecting the earth pressure coefficients, including backfill soil friction angle, ϕ, with different backfill-wall interface friction angle, δ, and horizontal seismic coefficient, α_h, are explored in detail for both active, k_a, and passive, k_p, earth pressure coefficients. The study shows an increase in both active and passive seismic coefficients with increase in horizontal seismic coefficient applied in opposite direction of backfill and reduction if the horizontal acceleration is applied in the direction of backfill.

Finally, seismic vulnerability of an abutment is investigated through extensive numerical simulation using incremental dynamic analysis (IDA) with 2D plane-strain finite element models of abutment-backfill system using ABAQUS subjected to a near field ground motion suite. This helps to incorporate the stochastic response of the abutment due to uncertainties in ground motions. As a final outcome of this study,

fragility curves are developed as a function of Peak Ground Acceleration at rock horizon. Fragility curves for different backfill-foundation combinations and with different friction angles and isotropic parameters are compared.

ACKNOWLEDGEMENT

First and foremost, I would like to express my gratitude to my supervisor **Prof. Yogendra Singh**, Department of Earthquake Engineering, Indian institute of Technology Roorkee for his continuous support and faith in me during different phase of my M.Tech. dissertation. His immense knowledge and frequent discussions throughout the work were extremely fruitful and helped me to overcome hurdles and problems I faced during this work.

I am highly obliged to **Dr. Dhiraj Raj** and **Ms. Bharathi M.** whose timely help and suggestions accelerated the thesis work. Their sincere guidance, criticism and appreciation encouraged me to be consistent throughout the thesis period without which the completion of the present work would not have been possible.

I am also thankful to **Mr. Modha Kavan Girishchandra** for his help in understanding of the concepts and moral support as a friend and mentor.

Scholarship given by **Ministry of Human Resources and Development**, Government of India is highly appreciated for this dissertation work.

I am also thankful to fellow students, juniors and seniors, their meaningful suggestions and support helped me in facing hurdles with confidence.

Further, I would like to acknowledge the extremely good computer facilities provided by the department without which this work would not have been possible.

Finally, I would like to thank my parents, **Mr. Sanjay Srivastava** and **Mrs. Seema Srivastava**, without whose beliefs, pursuing post-graduation would still have been a dream.

Thanks to everyone who has helped me in the completion of my thesis work.

Date: (Aman Srivastava)

TABLE OF CONTENTS

LIST OF FIGURES

LIST OF TABLES

Chapter 1 Introduction

1.1 General

Bridges, unlike buildings, are less redundant structural systems, which makes them more vulnerable in a seismic event as failure of a single structural component can cause severe damage and affect the functionality of the whole system. In the past, earthquakes in places like South America, Japan, New Zealand and California, bridges designed especially for seismic forces were critically damaged although the ground motion intensities they were subjected to was less than those specified by modern codes.

One of the reasons of this unexpected failure can be attributed to higher sensitivity of bridges to soil-structure-interaction, as compared to buildings. This increases even further due to the travelling wave effects subjecting the bridge to a non-synchronous input making its response more unpredictable.

Failure at abutment support is one of the reasons to impact not only the bridge system as a whole in major ground shakings, but also its functionality in smaller ones. This is attributed to:

1. Underestimation of the seismic earth pressure on abutment making it vulnerable to more forces and moment than those considered in design.
2. Settlement of the approach backfill soil causing abutment displacement and impacting the functionality of the bridge.

The response of the soil which is based on elastic theory or linear approach causes its participation to be low in the bridge system response to ground shaking. According to the observed damage, the geotechnical structures have increased amplification of the displacement due to soil effects (Rio Viscaya bridge,1990 Costa Rica earthquake) causing unexpected unseating (Nishinomiya-Ko bridge,1995 Kobe earthquake), lateral forces in deck, vertical ground settlement in the backfill as shown in Fig.1.1.

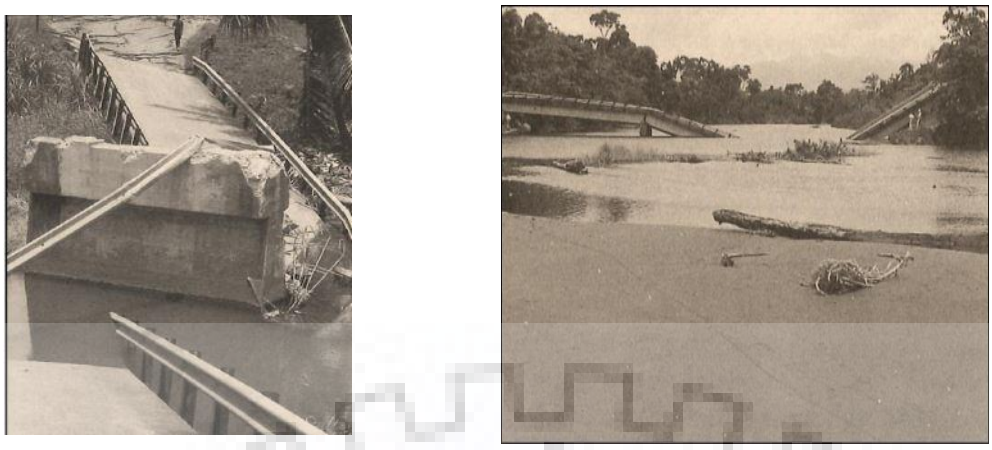

(a) (b)

Figure 1.1 Liquefaction failure, Rio Viscaya bridge, 1990 Costa Rica earthquake (Brando 2012).

Abutment slumping or rotation about wall and footing due to increase of earth pressure is rather common during earthquakes. Earthquake acceleration and impact of the bridge deck in the lateral direction are the reason for this high earth pressure. The movement of the deck in the longitudinal direction causes the abutment to rotate about its base towards the backfill which damages the back wall and concentrates the forces and moments at the base moreover the un-compacted soil has a tendency to flow with the failure soil (Rio Banano bridge,1990 Costa Rica earthquake).

(a) (b)

Figure 1.2 (a) Abutment slumping and rotation; and (b) Abutment failure due to passive pressure (Brando 2012).

Study of the effect of SSI on the structural system has been done for geotechnical structures like embankments, underground tunnels, retaining walls and abutments, pile

foundations etc. The response of a retaining structure is majorly studied in retaining walls but the same methodology can be applied for any type containment of soil.

Figure 1.3 Showa bridge failure (Liquefaction during Niigata Earthquake, 1964).

Figure 1.4 Pounding damage at the abutment 1995 Kobe earthquake (Brando 2012).

In the present dissertation, the gaps in the existing design of earth retaining structures have been investigated. The challenges in the coupled abutment-backfill system have been studied and finite element models (FEM) are developed to understand the earth pressure problem in detail. The results obtained through extensive numerical simulations

are then used to develop fragility curves to determine the vulnerability of a typical abutment in a seismic event.

1.2 Abutment- Backfill Coupled System: Challenges in Seismic Response

In the past, studies have been performed to determine the behavior of retaining structures through static, pseudo-static, pseudo-dynamic and time history analysis. One of the early studies on earth pressure by Mononobe-Okabe (M-O), based on coulombs theory, was given for seismic case using pseudo-static methodology in granular soils.

Mononobe-Okabe method was based on limit equilibrium theory, including the effect of earthquake inertial forces through static forces. Moreover, the analysis of the failure wedge was based on the following assumptions:

- Plane-strain condition was assumed i.e. end effects were neglected;
- The soil was cohesionless and assumed to be homogeneous throughout;
- The wedge is assumed to be plane;
- The displacements of the soil-wall system were in horizontal direction only;

These assumptions reduced the application of M-O method to conventional civil engineering problems of wall-backfill system and thus limits its use in real problems.

Later researchers have extended this to non-cohesive soils for both active and passive pressure (Caltabiano et al. 2000, 2012; Mylonakis et al. 2007; Shukla 2010; Soubra 2000). Empirical study of the SSI simulating the behavior of retaining walls due to soil non linearity has been done using Logarithmic-Spiral method, Finite Element solutions and Boundary Element method (Anoosh et al. 2007; Chouw and Hao 2005; Lee et al. 2004; Musharraf-uz et al. 1984; Olmos and Roesset 2008; Tokimatsu et al. 2005).

Major studies for simulating the behavior of wall-backfill system using Finite Element Method (FEM) (Al Atik and Sitar 2010; Beygi et al. 2018; El-Emam et al. 2004; Gharavi and Bargi 2012; Psarropoulos et al. 2005; Purkar and Kute 2015; Senthil et al. 2014; Tiznado and Rodriguez-Roa 2011; Xu et al. 2018; Zhu et al. 2018). Although these researches have closely simulated the response of wall to earthquake forces in form of equivalent static or non-linear dynamic analysis they lack to closely include the system components effect on the overall response of the wall-soil system.

In the last decade researchers have moved towards an approach to relate the backfill response to the functionality of the retaining system after an earthquake. Fragility curves have been used in buildings to determine damage probability corresponding to different damage states, thus giving an idea about their serviceability. Their use in retaining structures (Argyroudis et al. 2013, 2016; Sotiris et al. 2019) has been limited.

Figure 1.5 Field example of spill slope failure at a spill-through abutment at Cottonwood Creek, (Ettema et al. 2015).

1.3 Objectives of the Study

The aim of the present study is to understand the stochastic behavior of a retaining structure during a seismic event taking into account factors like topographic amplification, material damping, soil-structure interaction. The specific objectives of the present study include:

1. Numerical simulation of a classic seismic earth pressure problem of a horizontal backfill with vertical wall.
2. Computation of seismic earth pressure coefficients using pseudo-static approach.
3. Simulation of the coupled behavior of soil-abutment systems to estimate seismic capacity using Incremental Dynamic Analysis (IDA).

4. To estimate the fragility curves for the chosen abutments using the results of the Incremental Dynamic Analysis (IDA).

1.4 Methodology

In order to understand the concept of earth pressure, the most common problem of earth retaining structures was taken. The backfill was considered horizontal retained by a vertical wall. Finite element (FE) models of the problem have been developed using 2D plane strain quadratic element in ABAQUS (2016). The wall was modelled as a rigid beam to avoid its influence on the calculation of earth pressure coefficients. Backfill is taken as cohesion-less soil with sufficiently large boundaries to sustain the failure surface. The seismic force has been considered as pseudo-static force in terms of horizontal seismic coefficient, α_h. Further, the effect of variation in governing factors such as backfill soil friction angle, ϕ, with different backfill-wall interface friction angle, δ, on active and passive earth pressure coefficients have also been studied in detail.

In order to estimate the vulnerability of the abutment-backfill system extensive numerical study was performed using Incremental Dynamic Analysis (IDA) on 2D plane strain models. The stochastic behavior of the retaining wall due to variation in ground motion is taken into account. The results obtained were used in the development of fragility curves as a means to quantify the risk and damage induced during a seismic event of a particular peak ground acceleration (PGA). In the end a comparison has been made of the vulnerability of abutment retaining soil with different friction angle, ϕ, and different foundation soil.

1.5 Organization of Dissertation

Chapter 1 presents the basic introduction of the requirement of the present study, research and state of art of the designing of earth retaining structures, challenges in the abutment-backfill coupled system and objectives covered in the present thesis.

Chapter 2 presents a classic earth pressure problem for better understanding, determination of static and seismic earth pressure coefficients for active and passive case using pseudo-static methodology with variation in major governing factors including soil friction angle, ϕ, wall-soil interface angle, δ, and horizontal seismic coefficient, α_h.

Chapter 3 presents the modelling and analysis details used for the validation including mesh and geometry size and model boundary conditions.

Chapter 4 presents the non-linear soil parameters that are used in the further study for Incremental Dynamic Analysis (IDA).

Chapter 5 presents development of fragility curves using extensive numerical simulation using IDA on a 2D plane strain FE model. The developed fragility curves help in determining the seismic fragility of the abutment with its damage probability. Further, a comparison has been made between the damage probability of abutment retaining different backfill with two different foundation soil.

Chapter 6 summarizes the conclusions of present work. Further, recommendations for future work has also been outlined.

1.6 Novelty of the Work

- Displacement based approach is used to calculate static and seismic earth pressure coefficients.
- Actual distribution of seismic earth pressure and distribution of shear force and bending moment on the wall during a seismic event has been studied.
- Stochastic behaviour of the abutments has been studied using fragility curves and their comparison has been made for different backfills. In addition, effect of two different foundation soils has also been studied.

Chapter 2 Estimation of Seismic Earth Pressure

2.1 Introduction

Seismic earth pressure value and its distribution along the wall surface has always been of concern for (1) the estimation of seismic bearing capacity of shallow foundation, for example in skirt foundations, and well foundation; (2) analysis of plate and block anchors; and (3) for calculation of forces on bridge abutments and earth retaining structures.

In the past researchers have contributed to the development of an earth pressure theory, a solid design methodology to estimate the distribution and hence the amount of earth pressure and its point of application. Some of the earliest research has been done by Rankine, Mononobe-Okabe, Caquot, Sokolovski, for seismic earth pressure using pseudo-static, pseudo-dynamic and modified pseudo-dynamic method.

In pseudo-static analysis an equivalent static approach is used to take into account the inertial forces of the system induced during a seismic event. First used by Mononobe-Okabe, seismic earth pressure coefficients were calculated using a linear failure surface resulting in overestimation of passive and underestimation of active earth pressure. A better approach is to consider a curved failure surface (Kumar 2001; Morrison Jr. and Ebeling 1995; Shamsabadi et al. 2013; Subba Rao and Choudhury 2005). In pseudo dynamic approach the phase change of ground motion is taken into consideration but lacks damping characteristics of the backfill. In recent year (Pain et al. 2015; Rajesh and Choudhury 2017) have presented modified pseudo dynamic methodology to account for the backfill damping. The major shortcomings of the above mentioned studies is the assumption of a pre-defined failure surface except in some studies (Khatri 2019; Krabbenhoft 2018; Shiau et al. 2008) in which seismic coefficients were given using upper and lower bound limit analysis (FELA).

In the present study an attempt has been made to determine the static and seismic earth pressure coefficients using Force-displacement curves. Further, the variation of key parameters affecting the seismic earth pressure coefficients were studied in detail.

2.2 Problem Statement

A simple case of a retaining wall retaining horizontal backfill is considered. 2D plane strain finite element models (FEM) were prepared in ABAQUS. The study involves deduction of active and passive pressure coefficients for pseudo-static case. The coefficients are calculated by laterally pushing and pulling the wall towards and away from the backfill respectively.

The seismic case involves computation of K_a^+, K_a^-, K_p^+, K_p^- for active and passive coefficients distinguished on the basis of the movement of wall relative to horizontal seismic coefficient, α_h. In case of passive earth pressure coefficient positive superscript defines the movement of wall opposite to the direction of acceleration, K_p^+, and negative superscript designate movement of the wall towards the direction of acceleration, K_p^-. Similarly, in active positive superscript represents wall movement in direction of acceleration, K_a^+, and negative superscript for wall movement in opposite direction of acceleration, K_a^-.

2.3 Finite Element Modelling

Finite Element Modelling (FEM) is a numerical technique used to solve boundary value problems in engineering. However, it is an approximate method, its ability to handle very complex problems has made it popular. In FEM the system is divided into number of small elements which are inter connected to each other by a number of nodes. First, elemental stiffness matrix is generated for all the elements which takes care for the material properties and boundary conditions followed by the generation of mass matrix and applied force vector. By solving equations of motion, unknown displacements at each node is computed. But large number of discretized element create large number of equations of motion which requires highly efficient computer programs for the simulation of wave propagation problem.

2.3.1 Element and Meshing

2D finite element models (Fig.2.1) were prepared in ABAQUS using plane strain elements with quadratic geometric order (CPE8R). The retaining wall is modelled to be rigid, using beam element. Backfill soil was taken cohesion less and isotropic with Mohr-Coulomb failure criteria. The soil properties used in the study are given in Table 2.1.

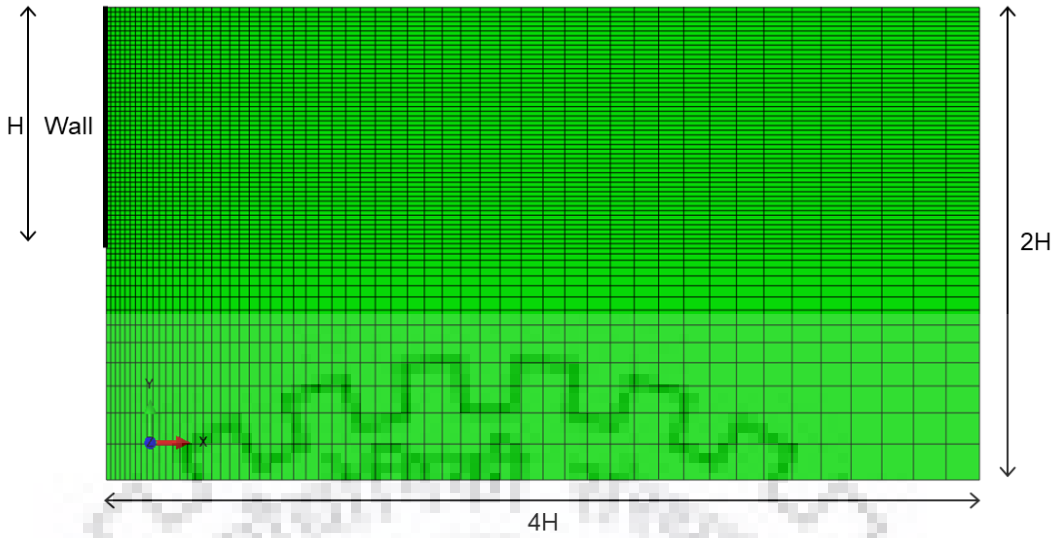

Figure 2.1 ABAQUS model of the retaining wall and backfill.

Table 2.1 Soil Properties used for Numerical Analysis.

Parameter	Value	Unit
Young's modulus (E)	437.4	MPa
Poisson's ratio (μ)	0.35	-
Internal friction angle (ϕ)	10 - 45	degree
Cohesion (c)	0.1	kPa
Unit Weight (γ)	18	kN/m^3
Material damping (ξ)	5	%
Ratio of wall friction angle to internal friction angle (δ/ϕ)	0 - 1	-

As ABAQUS uses Lagrangian finite elements, element spans -1 to +1, using the elements coordinate g and h shape function (interpolation function) is determined. The total number of elements in the FEM model were 3690, out of which 3640 were of quadratic quadrilateral elements (CPE8R) and 50 were linear line elements (B21). There are 2 types of elements used in the modelling:

1. The wall is modelled with a beam element B21 (a 2-node linear beam in a plane).
2. CPE8R (an 8-node biquadratic plane strain quadrilateral, reduced integration) elements are used to model the backfill soil.

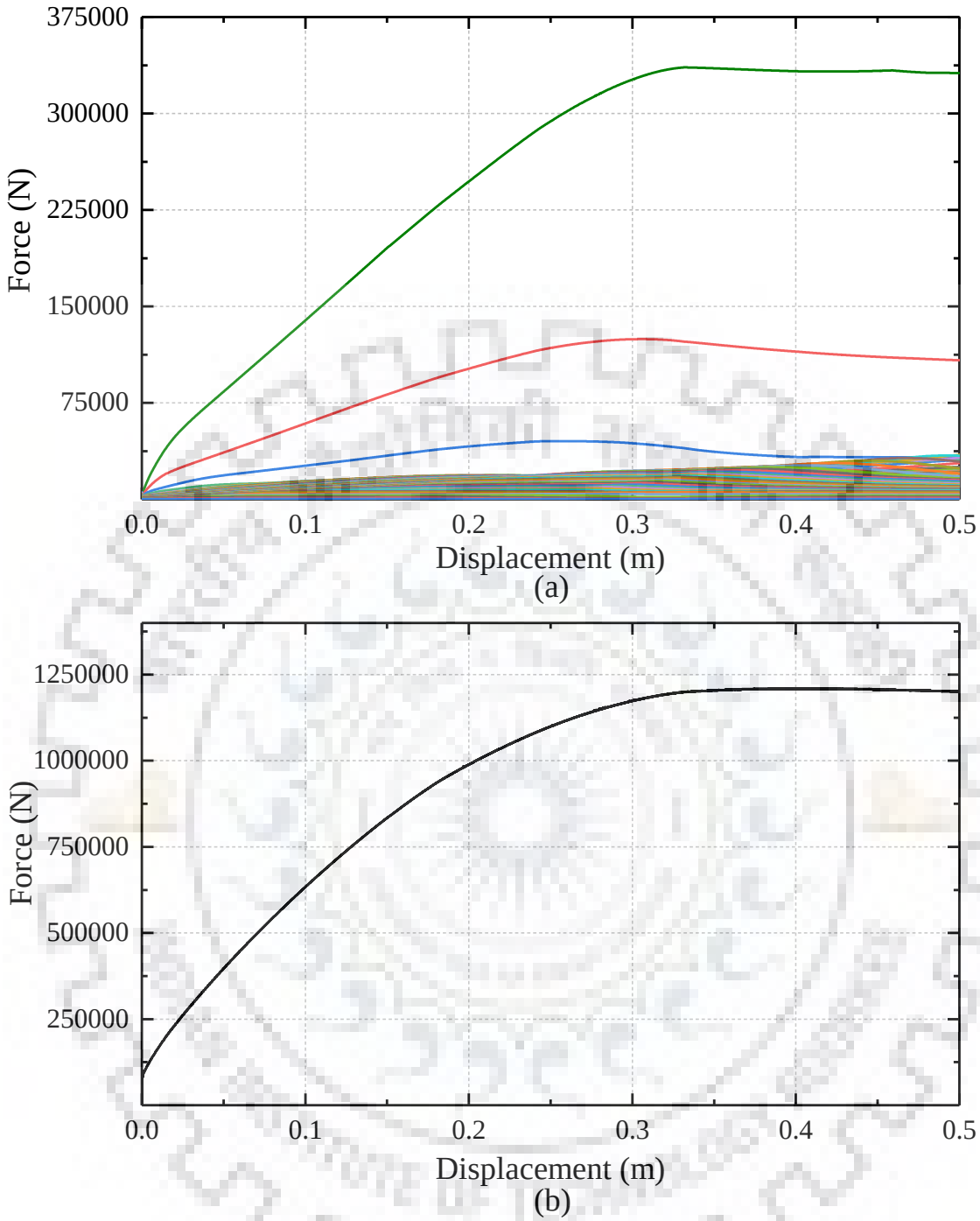

Figure 2.2 Load-displacement curve for (a) individual nodes (b) sum of all nodes of wall.

The boundary condition at the base of the model is assumed to be fixed with pinned at sides to allow movement only in vertical direction and restrict horizontal degree of freedom. The lateral boundary is taken sufficiently large to incorporate the failure wedge within limits and avoid boundary affect.

The reaction force-displacement curves generated by the movement of the wall with the soil on each node is summed up to get total force acting on the wall. The threshold

value of the total load displacement curve (Fig.2.2 (b)) thus obtained is then used to back calculate pressure coefficients. The distribution of this earth pressure behind the wall was taken triangular as given by Mononobe-Okabe:

$$P_a = \frac{1}{2}\gamma H^2 K_a, P_p = \frac{1}{2}\gamma H^2 K_p \tag{2.1}$$

P_a, P_p are the earth pressures, γ is the unit weight of soil and H is wall height (5 m).

The results are presented in this study for different δ/ϕ ratio where δ is the interface angle between the wall and the backfill and ϕ is the angle of friction of the soil.

2.4 Comparison with Past Studies

In the past researches have obtained earth pressure coefficients using (1) Plasticity theory (2) Method of characteristics (3) Upper and lower bound limit analyses; and (4) Upper and lower bound finite element limit analysis (FELA). In the present study force displacement curves generated from the reaction force on the wall were used to calculate earth pressure coefficients.

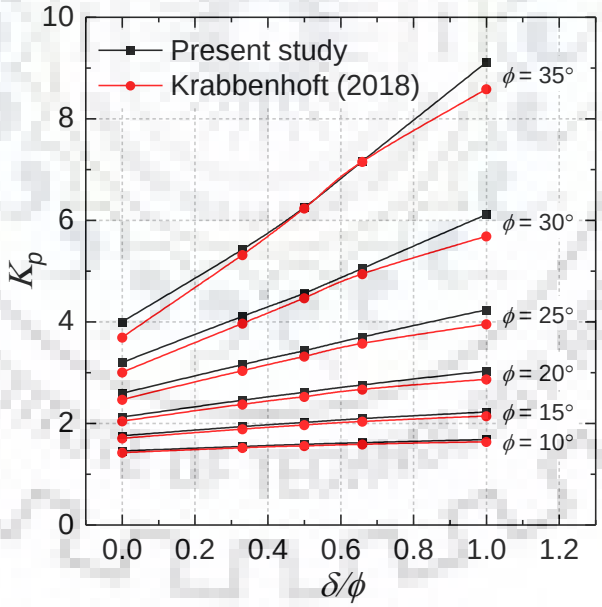

Figure 2.3 Comparison of the results given by Krabbenhoft (2018) and the present study for passive static case (α_h = 0).

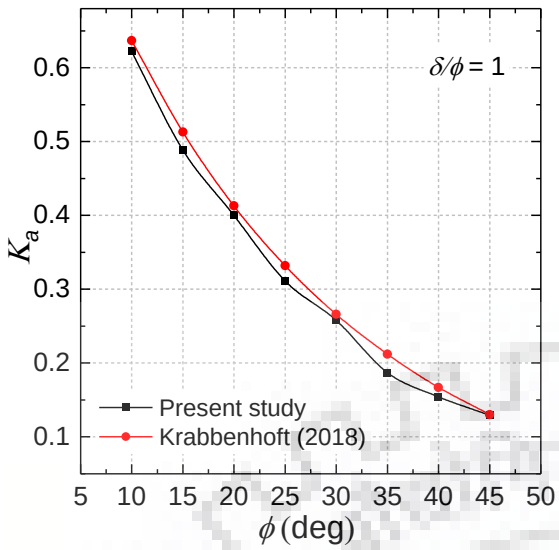

Figure 2.4 Comparison of the results given by Krabbenhoft (2018) and the present study for active static case (α_h = 0).

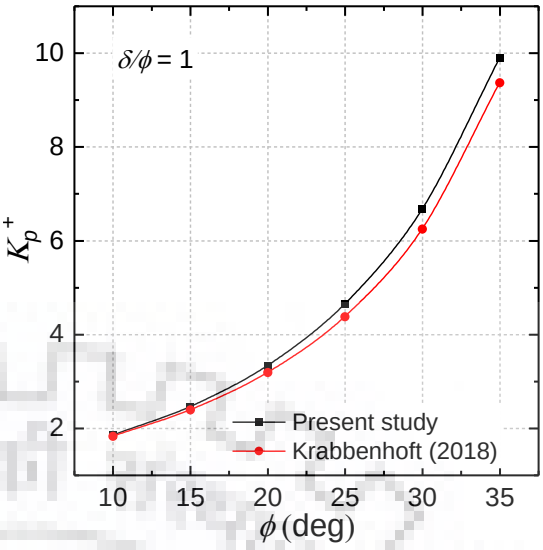

Figure 2.5 Comparison of the passive earth pressure coefficient given by Krabbenhoft (2018) and the present study for α_h = 0.15.

The values obtained were compared with the earth pressure coefficients given by Krabbenhoft (2018) (Figs. 2.3-2.5). Fig. 2.3 shows the variation of passive earth pressure K_p with wall-backfill interface friction angle for static case *i.e.* α_h = 0. Similarly, Fig. 2.4 shows active earth pressure coefficient varying with friction angle of soil and Fig. 2.5 shows seismic passive earth pressure coefficient obtained through pseudo-static analysis with horizontal seismic coefficient α_h = 0.15 in the direction opposite to wall movement K_p^+.

As can be observed from the comparison, the results obtained in the present study are slightly higher for passive earth pressure and slightly lower for active earth pressure coefficients. This is attributed to the fact that the coefficients provided by Krabbenhoft (2018) were obtained through FELA taking the average of coefficients obtained from upper and lower bound analysis, whereas, the finite element method used in the present study provides closer coefficients.

2.5 Result and Discussion

The effect of different governing factors, friction angle of soil, ϕ, wall-backfill interface angle, δ, and horizontal seismic coefficient, α_h, on earth pressure coefficient has been studied in detail. For this purpose, extensive numerical analysis has been performed by

varying soil friction angle, ϕ, from 10° to 45° with ratio of wall friction angle, δ, to ϕ varying from 0 to 1. The horizontal seismic coefficient, α_h, was varied in pseudo-static analysis from 0 to 0.3 with an increment of 0.05.

A structural design engineer is interested in the forces and moments applied on the structure. Although, the distribution of the static and dynamic earth pressure is taken to be triangular and dynamic increment as rectangular, an approach has been made to determine and compare their distribution along the wall height. Fig. shows the distribution of earth pressure using pseudo-static methodology results for a few cases ($10k_a^+$, $10k_p^+$, $20k_p^+$) with varying horizontal seismic coefficient (α_h = 0.1 and 0.2) and wall-backfill interface angle to friction angle ratio (δ/ϕ = 0 and 1).

Results of the parametric study have been shown in Figs. 2.6 - 2.10. The following observation can be made from the results:

1. It has been observed that passive seismic earth pressure coefficient, K_p^+ corresponding to wall movement opposite to the direction of acceleration, gradually increases and passive seismic earth pressure coefficient, K_p^- corresponding to wall movement in the direction of acceleration, gradually decreases with the increase in horizontal seismic coefficient.
2. It has also been observed that active earth pressure coefficients, K_a^+ for wall movement in the direction of acceleration, gradually increases and active earth pressure coefficients, K_a^-, for wall movement in the opposite direction of acceleration, gradually decreases with the increase in horizontal seismic coefficient.
3. It has been found that with increase in soil friction angle, ϕ, and backfill-wall interface angle, δ, both passive pressure coefficients (K_p^+, K_p^-) increase.
4. It has also been found that with increase in soil friction angle, ϕ, and backfill-wall interface angle, δ, both active pressure coefficients (K_a^+, K_a^-) decrease.
5. In presence of seismic loading (as horizontal seismic coefficient), the active and passive pressure envelops are distributed in trapezoidal form along the height of wall as shown in Fig. 2.6.
6. In presence of gravity loading only, the active pressure envelop is distributed in triangular pattern along the height of wall as shown in Fig. 2.6 (b).

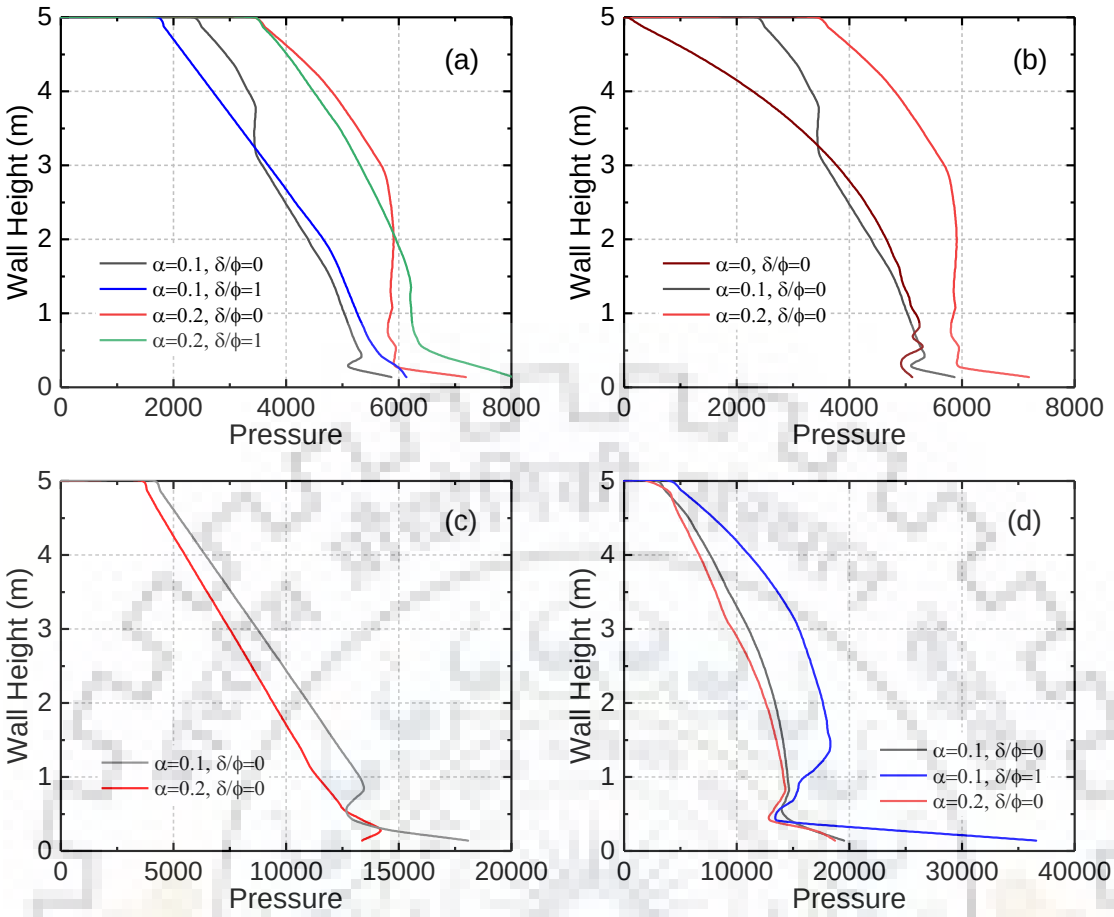

Figure 2.6 Pressure distribution envelop for (a) active earth pressure with ϕ = 10° , α_h = 0.1 and 0.2 and δ/ϕ = 0 and 1; (b) active earth pressure with ϕ=10° , α_h =0, 0.1 and 0.2 and δ/ϕ = 0; (c) passive earth pressure with ϕ = 10° , α_h = 0.1 and 0.2 and δ/ϕ = 0; and (d) passive earth pressure with ϕ = 20° , α_h = 0.1 and 0.2 and δ/ϕ = 0 and 1.

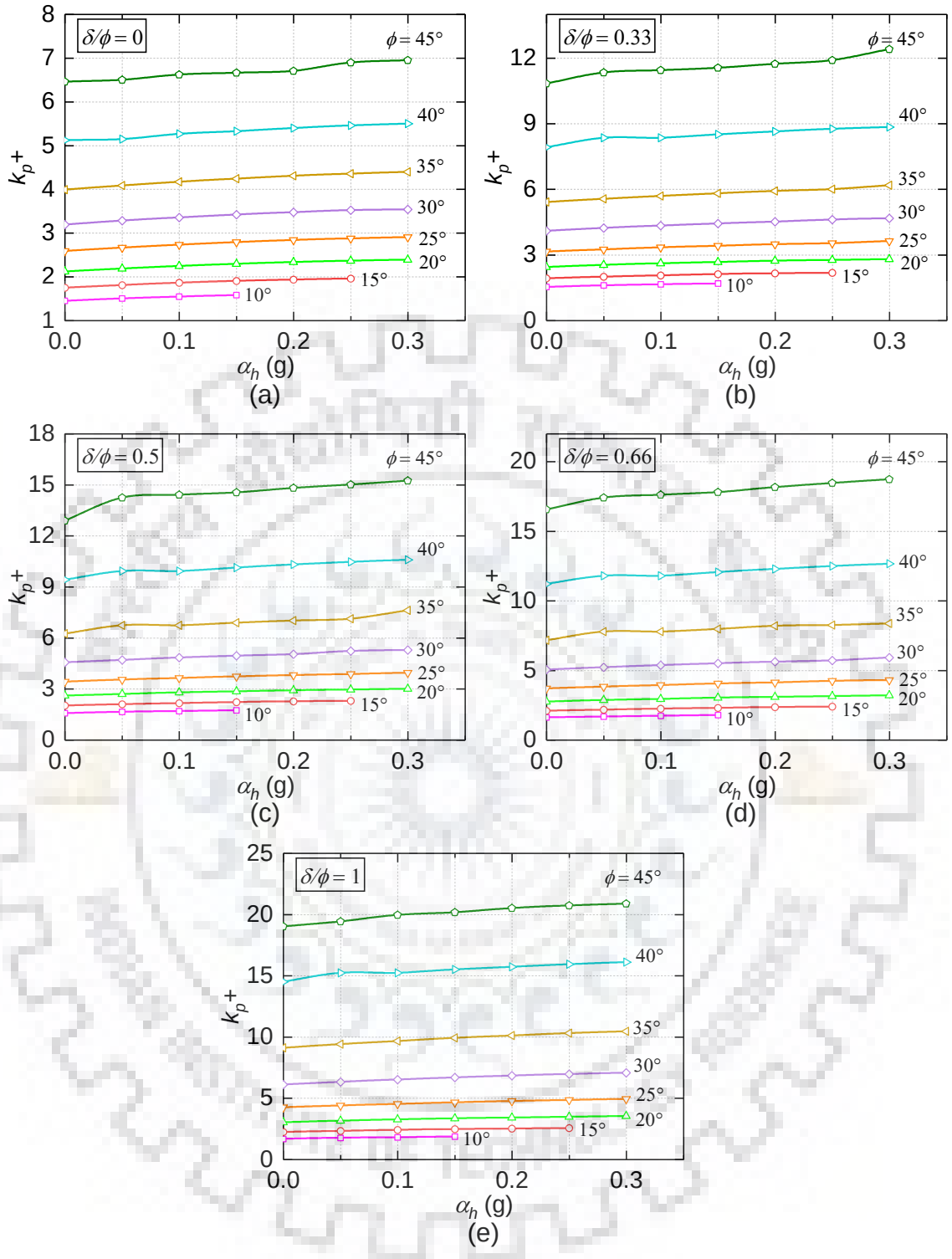

Figure 2.7 Passive earth pressure coefficient K_p^+ for wall movement opposite to the direction of acceleration with friction angle, ϕ, varying from 10° to 45° for (a) $\delta/\phi = 0$; (b) $\delta/\phi = 1/3$; (c) $\delta/\phi = 1/2$; (d) $\delta/\phi = 2/3$; and (e) $\delta/\phi = 1$.

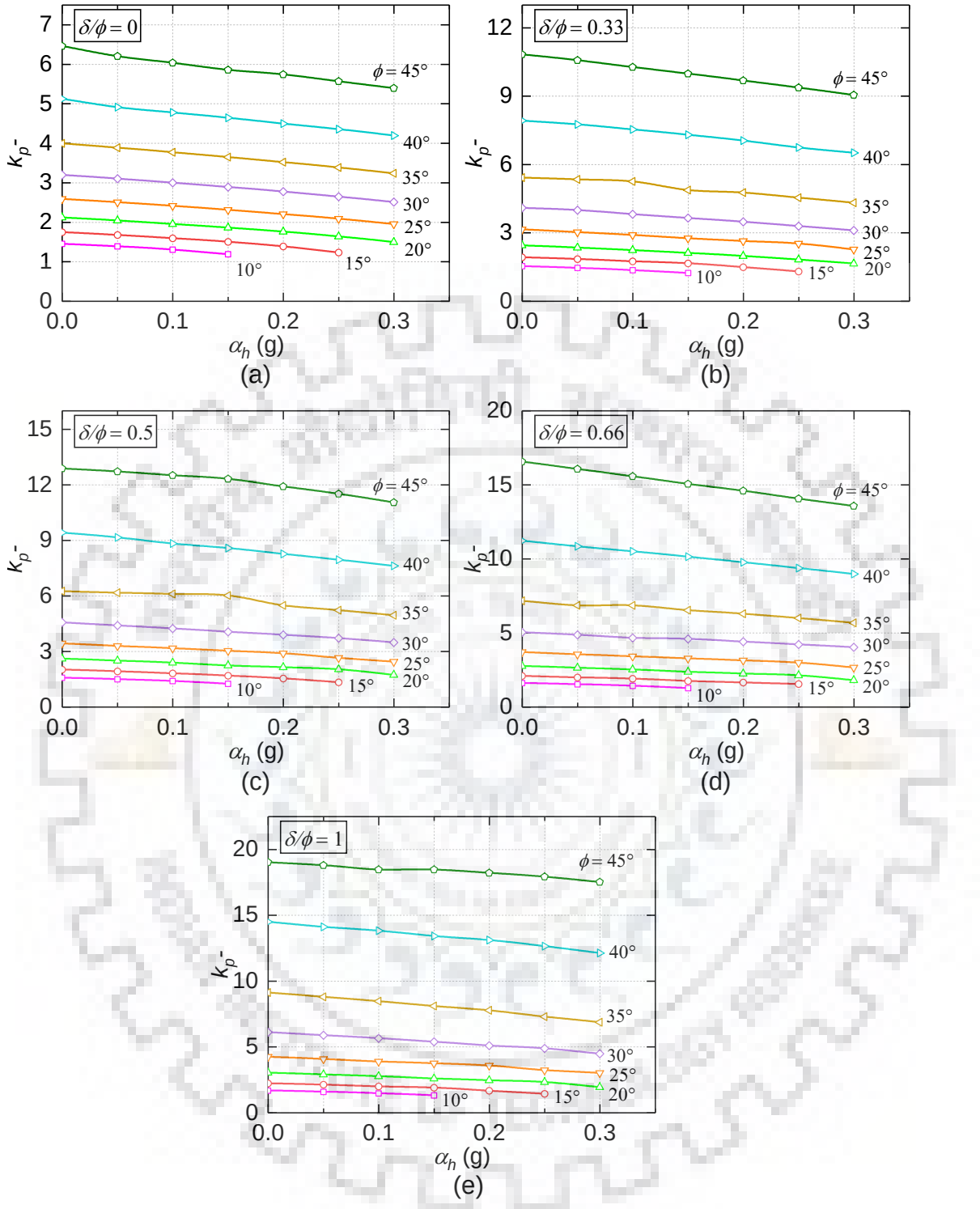

Figure 2.8 Passive earth pressure coefficient K_p for wall movement in the direction of acceleration with friction angle, ϕ, varying from 10° to 45° for (a) $\delta/\phi = 0$; (b) $\delta/\phi = 1/3$; (c) $\delta/\phi = 1/2$; (d) $\delta/\phi = 2/3$; and (e) $\delta/\phi = 1$.

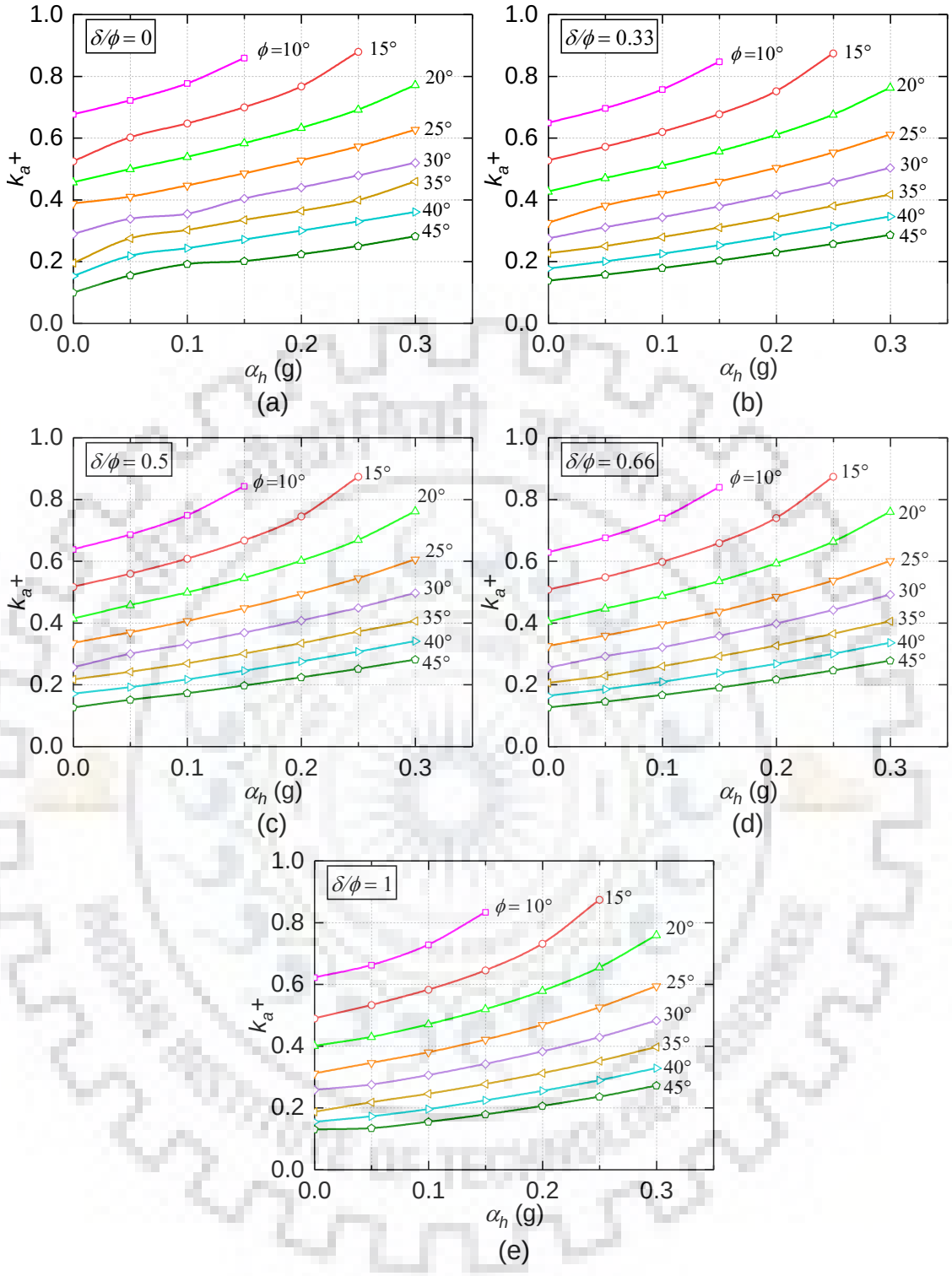

Figure 2.9 Passive earth pressure coefficient K_a^+ for wall movement in the direction of acceleration with friction angle, ϕ, varying from 10° to 45° for (a) $\delta/\phi = 0$; (b) $\delta/\phi = 1/3$; (c) $\delta/\phi = 1/2$; (d) $\delta/\phi = 2/3$; and (e) $\delta/\phi = 1$.

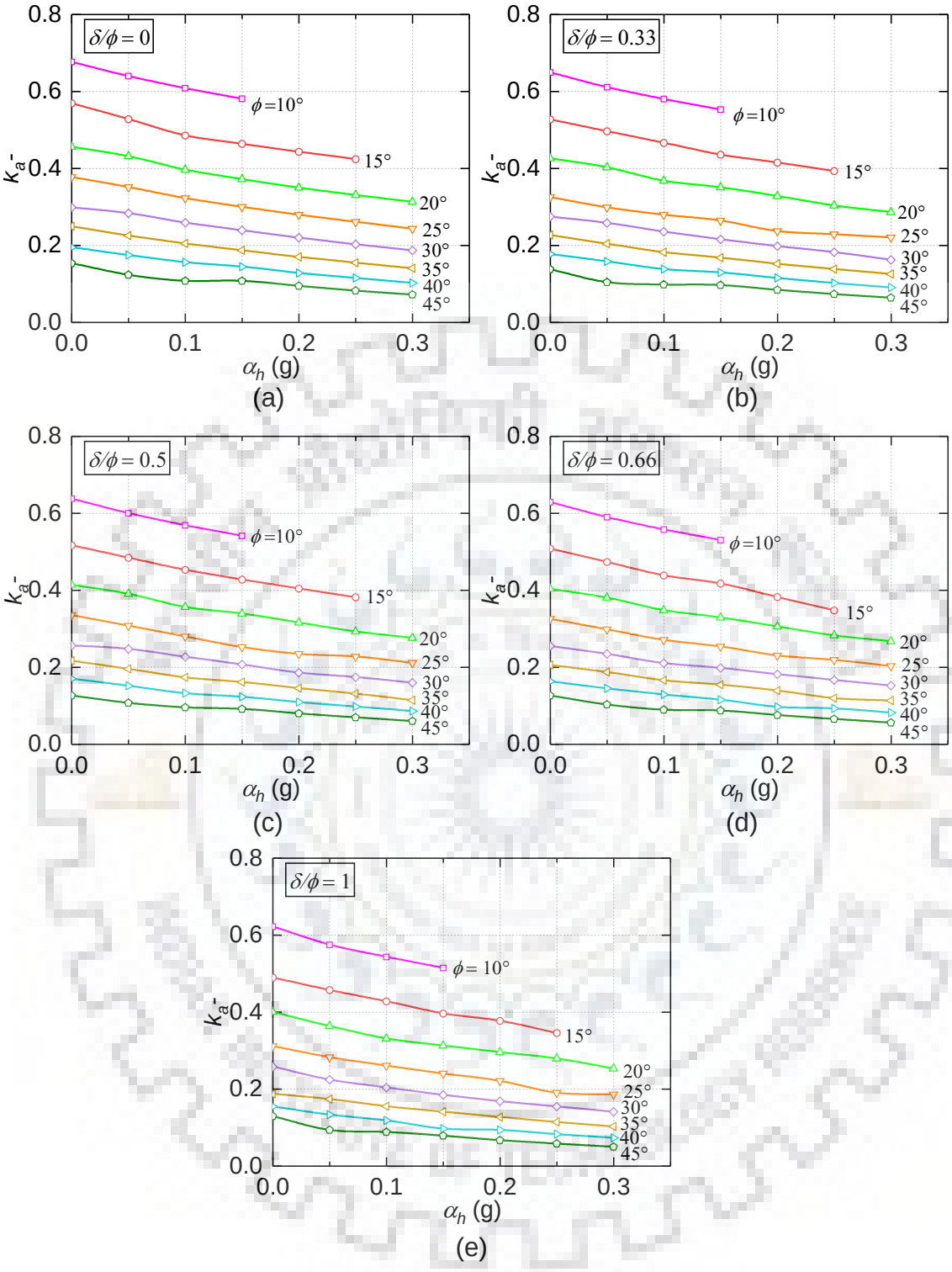

Figure 2.10 Passive earth pressure coefficient K_a^- for wall movement opposite to the direction of acceleration with friction angle, ϕ, varying from 10° to 45° for (a) δ/ϕ = 0; (b) δ/ϕ = 1/3; (c) δ/ϕ = 1/2; (d) δ/ϕ = 2/3; and (e) δ/ϕ = 1.

Chapter 3 Modelling and Analysis of Soil-Abutment System

3.1 Introduction

In the past, there has been a lot of studies and vast area has been explored in the designing of earth retaining structures for soil pressure forces and moments. Although there is availability of immense amount of documents and design codes dedicated for this purpose, there is still a scope for further research. There has been an issue regarding the distribution of seismic earth pressure along the height, first developed by Mononobe-Okabe, through pseudo-static approach and has been followed in the current designs of abutments, retaining walls, embankments, pile and shallow foundations.

The pseudo-static approach has its own limitations and assumptions which make its application restricted to a subset of common civil engineering problems. For example, the seismic coefficient is taken constant throughout the backfill. In actual seismic event, there would be amplification of the ground motion as it propagates through the soil mass. Moreover, it has been observed that the distribution of the seismic earth pressure varies from the triangular distribution considered in current design practice.

These gaps in the past studies suggest that there is a requirement of a more realistic approach in order to find out the actual distribution and point of application of seismic earth pressure. A better approach can be through non-linear time history analysis (NLTHA) taking into account the amplification of ground motion, material damping, layered soil and strength reduction. Researchers (Argyroudis et al. 2013; Pitilakis et al. 2014a; Sotiris et al. 2019; Zamiran and Osouli 2018b) in their studies have developed fragility curves in order to quantify the vulnerability of retaining structures during a seismic event using Incremental Dynamic Analysis (IDA).

This chapter presents the geometry and soil profile to be used for the validation of the methodology. Further, for the purpose of novelty of the present work modifications in the soil modelling, such as incorporating soil nonlinearity, has been done. A bridge abutment is modelled in a simplified manner with a cantilever retaining wall on a surface foundation as shown in Fig.3.1. Height of the abutment, H, commonly used in practice, equal to 6 m is considered. The superstructure is assumed to rest on bearing on the abutment and with no horizontal forces. A vertical load of 200 kN/m is applied on top of the abutment in order to account for dead load of deck.

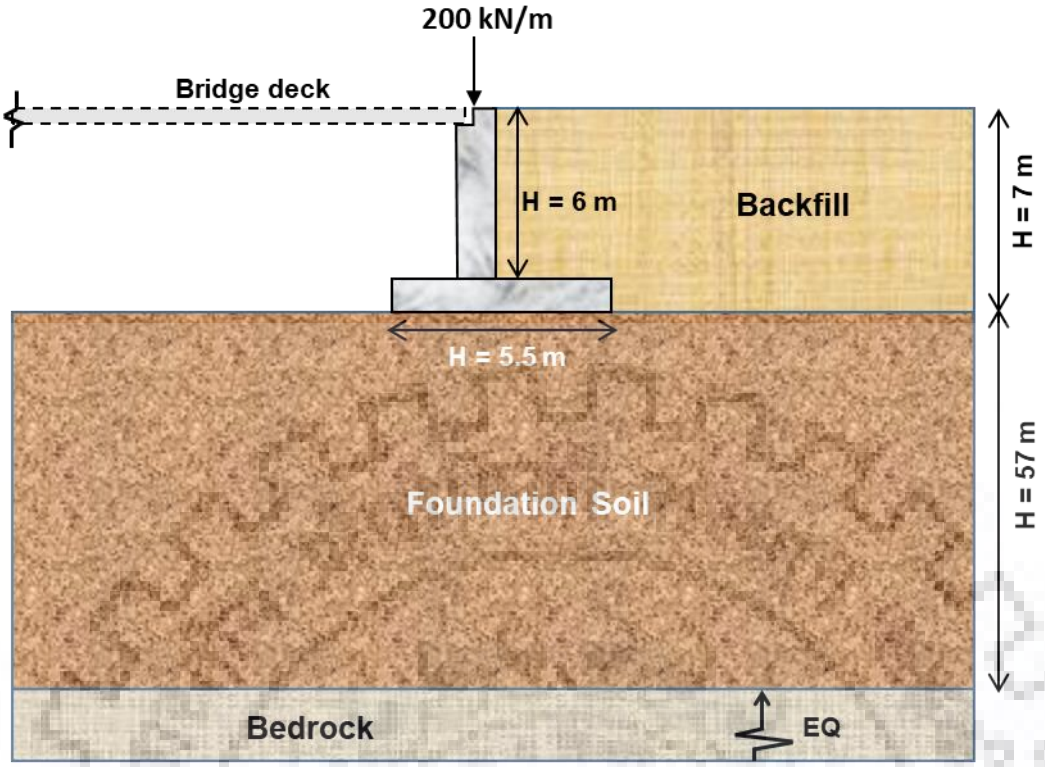

Figure 3.1 Geometry of the abutment under study.

In the present study an attempt has been made using 2D finite element models developed in ABAQUS to estimate the vulnerability and the forces and moments generated in an abutment. For this purpose, fragility curves have been developed using IDA and a comparison has been made for the probability of damage for different backfill soils with two different foundations. In the end for the completeness of the framework distribution of bending moment and shear force on the abutment during a seismic event has been studied.

3.2 Finite Element Modelling

In this chapter dynamic behavior of the abutment-backfill coupled system is studied using a 2D FE model prepared in ABAQUS. A series of finite element analysis were performed to get the dynamic response of the system. All the models were conducted in two stages- first step was static, general to account for the in situ stresses and equilibrium under gravity. Second step was dynamic implicit in which non-linear time history analysis is performed.

3.2.1 Element and Meshing

As the FEM is an approximate numerical method, accuracy of the results depends on the fineness of the mesh considered in the model. As suggested by (Kuhlemeyer and Lysmer 1973), maximum size of the element should be limited to $\lambda/_8$ to $\lambda/_{12}$ for wave propagation problem, where, λ is wavelength of input motion obtained by the ratio of shear wave velocity to the predominant frequency of the motion. In present study, force displacement curves are obtained by different mesh sizes to see the convergence of the results for particular model. Although the change was minimal with change of elements to nearly 1/3rd because of the use of quadratic elements instead of linear. From this parametric study mesh size of $\lambda/_{10}$ is used for the model.

Mirror modelling has been done to simplify the boundary effects and to account for the asymmetry of the accelerograms applied (Garini et al.). There are 2 types of element used in the modelling:

1. The wall is modelled with a plane strain element of CPE8R element type.
2. CPE8R an 8-node biquadratic plane strain quadrilateral, reduced integration is used to model the backfill soil in the close proximity of the abutment where major stress strain will occur.
3. At a far of distance from the major stress strain region 4-node bilinear plane strain quadrilateral, reduced integration CPE4R. The mesh farther away from the wall is modelled with a coarser mesh to reduce the computation time.

The total number of elements generated were 20790, 4388 of them were quadratic quadrilateral elements of type CPE8R and 16402 linear quadrilateral elements of type CPE4R. The soil backfill was divided into 4 layers and the footing soil was divided into 10 layers. The meshing was taken so as to keep the maximum element size from *λ/8* to *λ/12* for each layer.

3.2.2 Boundary Conditions

As the earth mass is infinite in extent, for wave propagation problem, an infinite system needs to be studied. Finite element modelling of such a system is practically impossible as the computational effort required will be very large. In order to simulate an infinite system, proper artificial boundary needs to be modelled to avoid the reflections from the ends. Therefore, absorbing boundaries which absorb the seismic wave energy and avoid

reflections or transmitting boundary needs to be used which will allow the waves to propagate. In the present study following boundary conditions are used:

3.2.2.1 Fixed Base

Fixed base is the reflecting type of boundary where directly acceleration time history can be applied. Reflections from the base generates some periodic motion at the top of the model.

3.2.2.2 Parasitic Boundary

Parasitic boundary condition is applied at the lateral ends of the model to avoid bending failure of the soil mass. Left edge node is connected with pin to the corresponding node in the mirror model on the right to ensure equal displacement of both the nodes (Sextos et al. 2017). Pin connection of the left edge node to the right edge node ensures shear failure mode of the soil column.

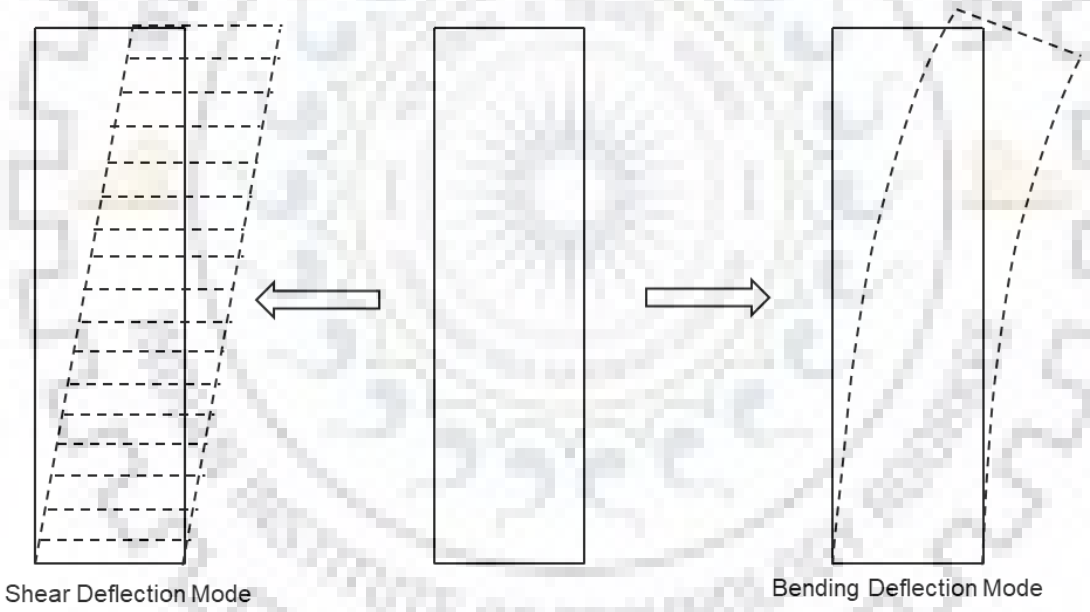

Figure 3.2 Shear and bending deflection modes of soil column (Modha 2018).

Argyroudis (2013) in his study developed fragility curves for bridge abutment taking two backfill resting on two different types of foundation soil (type C and type D). For the development of these curves PGA was taken as the intensity measure (IM) parameter and the peak vertical ground displacement (PVGD) of the backfill was taken as the damage index. Incremental dynamic analysis (IDA) was performed to determine the uncertainty in ground motion (β_D). Five acceleration time histories were taken for 2D

coupled system analyses scaled from 0.1g to 1g. The details of the ground motions used are shown in Table 3.1.

Table 3.1 Details of Ground Motion used for Validation.

Earthquake	Year	Station	Moment Magnitude, M_w
Koaceli, Turkey	1999	Gebze	7.4
Hector Mine, USA	1999	Hector	7.1
Parnitha, Greece	1999	Kypseli	6.0
Loma Prieta, USA	1989	Diamond Height	6.9
Umbria Marche, Italy	1998	Gubbio-Piana	4.8

3.2.3 Soil Profiles and Geometry

Two foundation soils (type C and type D) were considered in the study performed by Argyroudis (2013) and henceforth the same foundation profile has been used in the current study. An initial value of undrained shear strength C_o is assumed at the surface and varied along the depth of the foundation as a function of overburden pressure, σ_n, at any layer n. Shear modulus is estimated as a function of undrained shear strength, C_o, multiplies by a constant, α, whose value depends on the type of soil. The parameters used in soil modelling are given in Table 3.2. The variation of G_{max} with depth of foundation is shown in Fig. 3.3.

Table 3.2 Soil Parameters for Foundation Soil.

Parameter	Value
Density, (γ)	19.25 kN/m^3 (Type C)
	18.25 kN/m^3 (Type D)
Poisson's ratio, (μ)	0.35
Undrained shear strength, C_o	50 kPa (Type C)
	20 kPa (Type D)
Undrained shear strength variation, C_n	$C_n=C_o+0.25\sigma_n$
Shear modulus variation, G_{maxn}	$G_{maxn}=\alpha C_o$
Constant, α	1000 (Type C)
	800 (Type D)

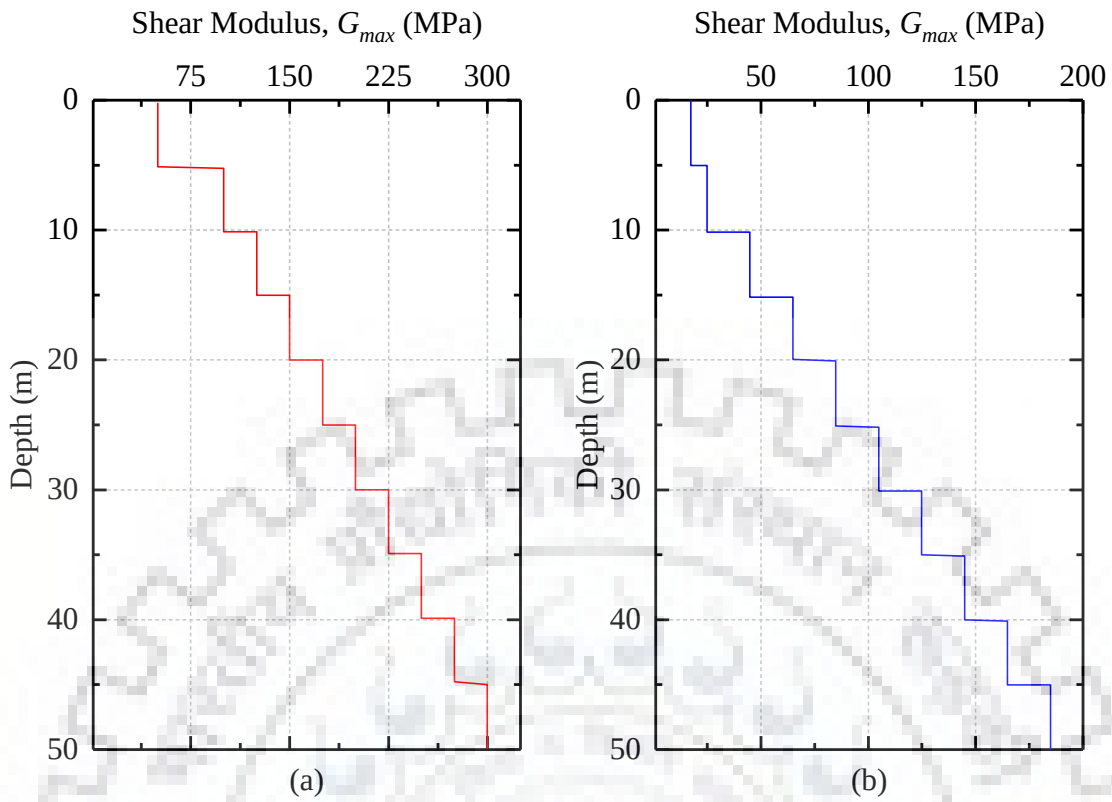

Figure 3.3 Variation of shear modulus, $G_{max,}$ along depth of foundation **(a)** Type C **(b)** Type D.

In order to account for the shear modulus reduction 1D equivalent linear ground response analysis was performed. The results from 1D equivalent linear analyses with ground motion scaled at 0.1g was used to account for the variation of shear modulus and damping with yield strain. A corresponding average reduction in *G* value is taken (0.68 for soil type C and 0.55 for soil type D) for the soil in 2D analyses. This assumption is valid for small strain conditions in which equivalent linear approach can be applied for higher strain Mohr – Coulomb yield criterion is employed. The backfill soil properties and G_{max} variation is as given in Table 3.4 and Fig.3.7:

Table 3.3 Soil Parameters for Backfill Soil.

Parameter	Value
Density, γ	18 kN/m^3 (backfill 1) 19 kN/m^3 (backfill 2)
Friction angle, ϕ	36^o (backfill 1) 40^o (backfill 2)

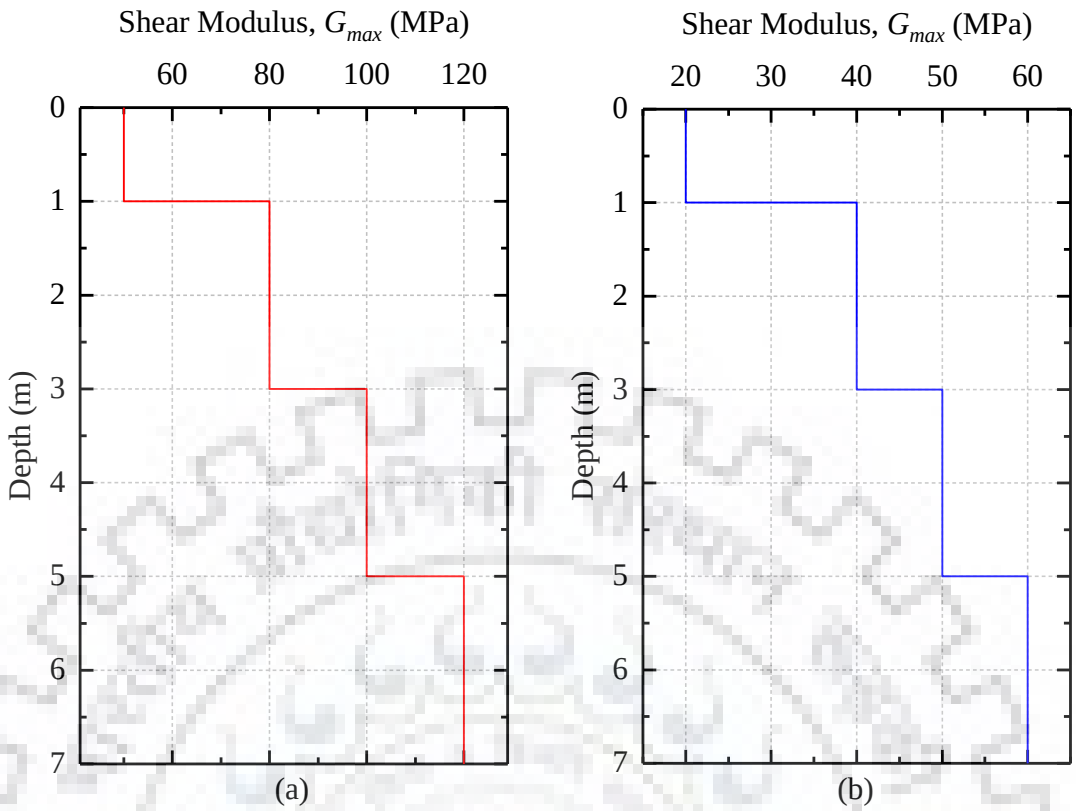

Figure 3.4 Variation of shear modulus G_{max} along depth of backfill (a) Soil type C (b) Soil type D.

The geometry of the model consists of quadratic plane strain element in the vicinity of expected stress and strain accumulation *i.e.* near the wall soil interaction region and linear plane strain elements away from the region under consideration as shown in Fig. 3.4. This helps in reducing computation time without compromising with the accuracy of results.

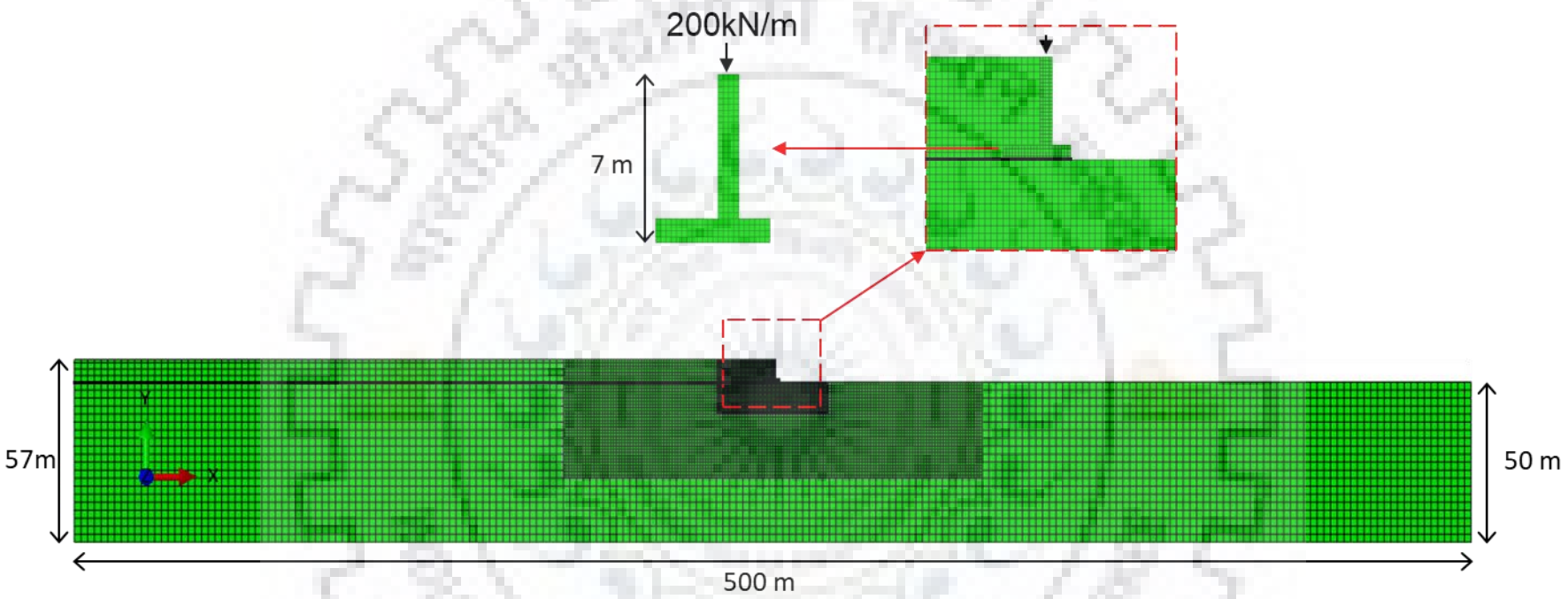

Figure 3.5 2D Finite element model prepared in ABAQUS.

3.3 Ground Response Analysis

Ground response analysis involves study of the response of soil to earthquake ground motion to develop site specific spectra and determine the forces induced by ground shaking which may result in liquefaction and landslides. It is generally analysis of amplification in ground motions as it propagates from bed rock to the surface.

Propagation of ground motion wave is not exactly vertical. The waves generate from rupture plane and gets transmitted in all the directions and gets reflected and refracted as it propagates. Soil at shallow depths have lower wave propagation velocity compared to the soil beneath causing the wave to be bent in a nearly vertical direction. Due to the near vertical propagation of wave near the surface ground response analysis is done taking 1D wave propagation with the horizontal soil layers to be assumed of infinite extent in both the direction. Development of the transfer function is crucial for ground response analysis. Uniform damped soil with rigid base boundary was used for the development of the transfer function for the soil properties to be used further for analysis. For this study ground motion Koaceli is used.

The ground motion with PGA scaled to 1g was de-convoluted to the depth of the model using DEEPSOIL and the ground motion obtained at the base was applied at the base in ABAQUS with model of the same soil properties and allowed to propagate to the top.

Transfer function is developed through the ratio of the response Fourier amplitude at the surface to the base and is a plot of the amplification factor with the frequency. The numerical results were compared with the analytical formulae for uniform, damped soil with rigid base given as:

$$\left|F_2(\omega)\right| \approx \frac{1}{\sqrt{\cos^2 kH + (\xi kH)^2}} = \frac{1}{\sqrt{\cos^2(\omega H/v_s) + \left[\xi(\omega H/v_s)\right]^2}} \qquad (3.3)$$

The frequencies at which the transfer function attains a peak value are corresponding to natural frequencies of the soil.

3.3.1 Comparison of Ground Response

The response spectra of the ground motion applied at top of DEEPSOIL was compared with the response spectra of the ground motion obtained at top of ABAQUS model as shown in Figure 3.5. The analytical results of the transfer function obtained through numerical analyses was compared with the analytical formulae.as shown in Figure 3.6.

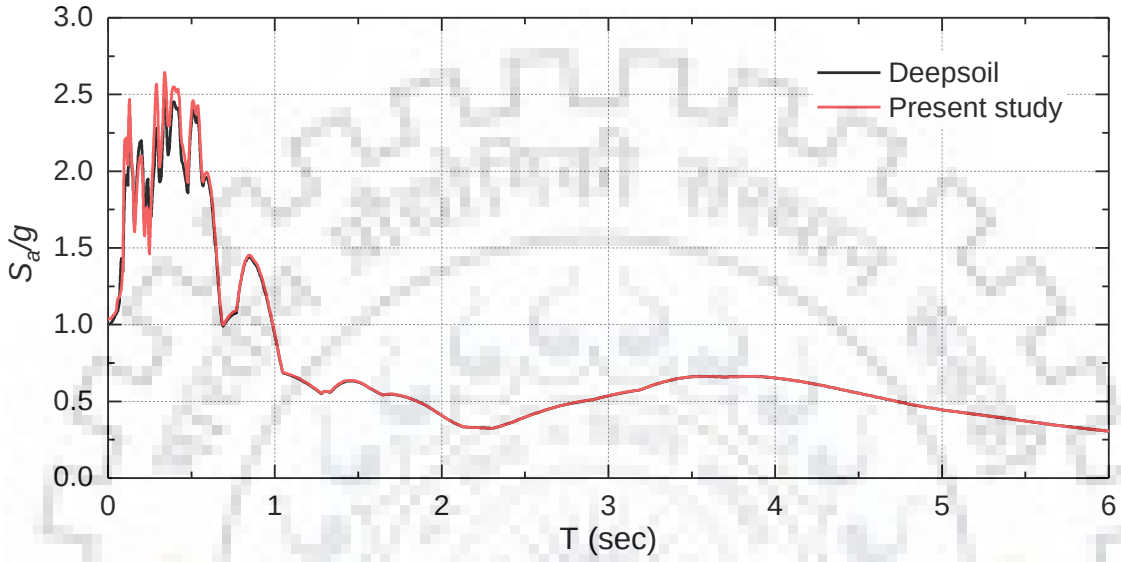

Figure 3.6 Comparison of the response spectra of ground motion (Koaceli) at the ground surface, obtained using equivalent linear 1-D wave propagation (DEEPSOIL) and Finite element analysis (ABAQUS) (Present study).

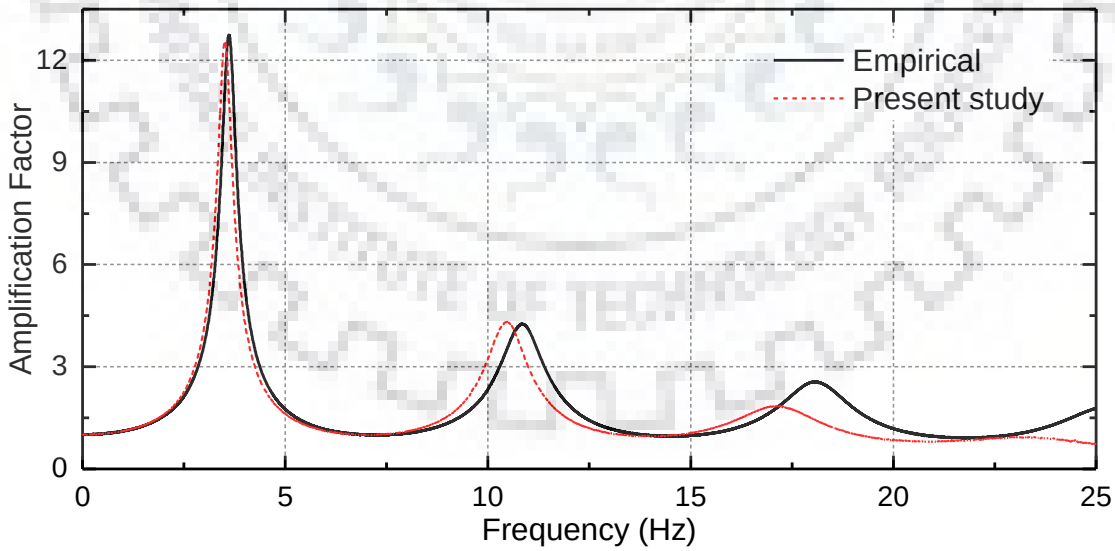

Figure 3.7 Comparison of the transfer function obtained with analytical formula and through Finite element analysis of ground motion (Koaceli).

3.4 Validation

In order to validate the numerical modelling, the response given by the study of Argyroudis (2013) in terms of peak vertical ground displacement (PVGD) performed using PLAXIS has been compared with the results obtained through 2D plane strain models developed in ABAQUS. The foundation soil details discussed earlier in this chapter were used along with two different cohesion-less backfills

The comparison of the response in terms of peak vertical ground displacement of the backfill obtained in study by Argyroudis (2013) and through the adopted methodology in present work is shown in Fig.3.7. The ground motions used in the study by Argyroudis (2013) were applied at the bedrock. The results given in the study were in terms of Incremental dynamic analysis (IDA), with increase in PGA, the response of the system in terms of backfill settlement or vertical displacement is used as the demand parameter to quantify the abutment-backfill system response. Henceforth, the same methodology is used to study the variation in response of the system retaining soil with different friction angles and resting on different foundations when subjected to different scaled ground motions. A detail study is also performed to study the bending moment shear force distribution in the wall and to generate capacity curves for the system.

An attempt is made to take forward the framework generated by Argyroudis (2013) in his study for fragility curves of abutments. For this purpose, the soil non-linearity is taken into account for the backfill as well as the foundation soil. Three different backfills with varying shear wave velocity along the depth and with different friction angle (ϕ = 30˚, 35˚, 40˚) and density (γ = 17, 18, 19 kN/m^3) were used in combination with two foundation soil (Type C and Type D). The backfill were modelled as cohesion-less whereas the variation of cohesion in the foundation is taken as a function of overburden pressure. A suite of scaled ground motions was used and response of a 2D finite element model prepared in ABAQUS was obtained.

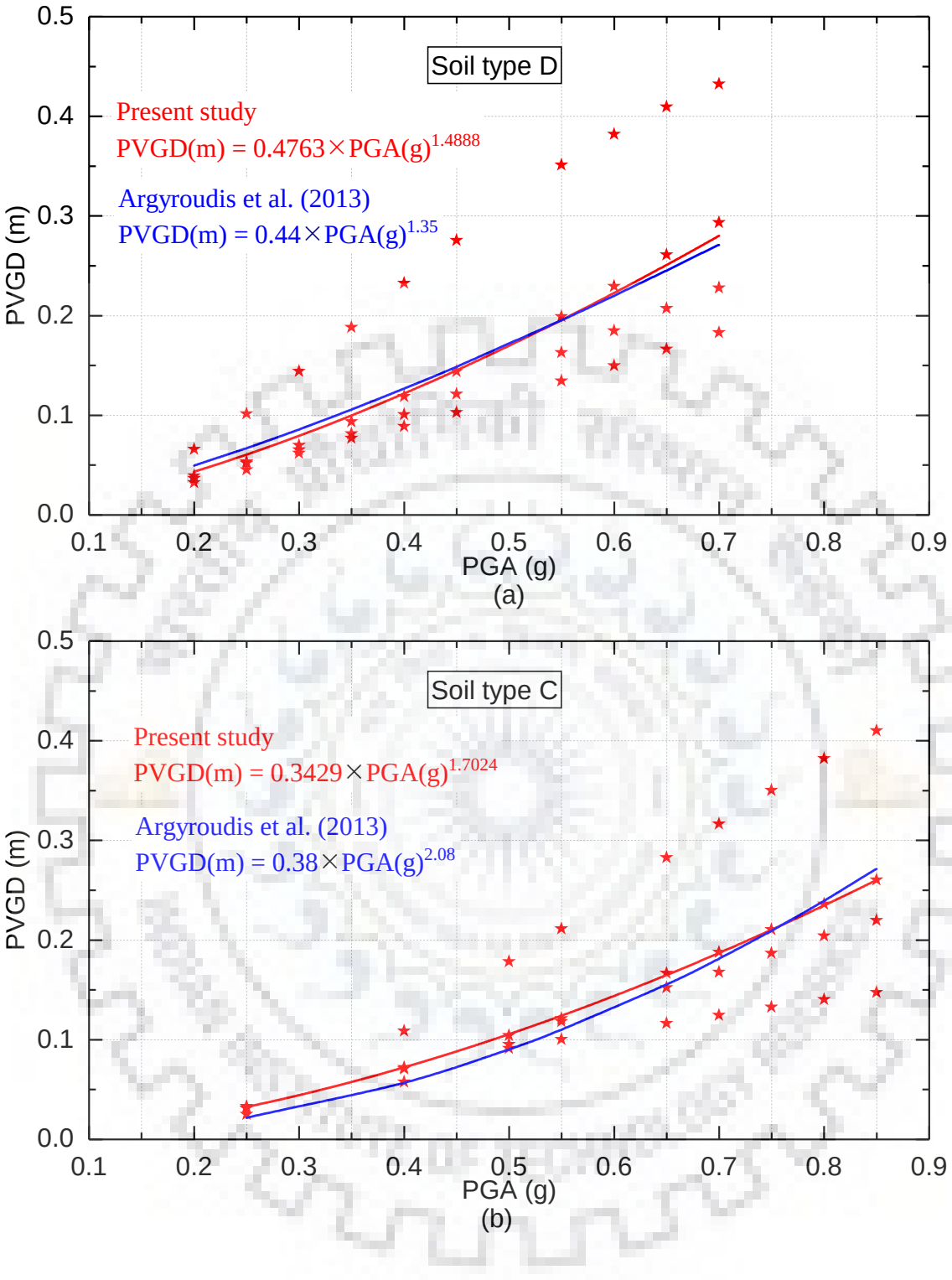

Figure 3.8 Comparison of results obtained in present study with those obtained by Argyroudis (2013) for backfill 1 resting on foundation (a) Type D; and (b) Type C.

Chapter 4 Nonlinear Dynamic Analysis

4.1 Nonlinear Modelling of Soil

Soil has been known to behave non-linearly with increase in shear strain. A reduction in the shear modulus along with an increase in material damping has been observed in the past studies. Small strain shear modulus is related with small shear velocity given as:

$$G_{\max} = \rho V_s^2 \tag{4.1}$$

where, ρ is the mass density of the soil. Shear modulus is simply the slope of the shear stress strain curve. A clear relationship between the parameters shear modulus, *G*, shear strain, γ, shear stress, τ, and damping, *D*, is illustrated in Fig.4.1. Damping may be defined as the ratio of energy dissipated in one cycle, W_D, to the total strain energy stored in the system also known as hysteretic damping given as

$$D = \frac{1}{4\pi}\frac{W_D}{W_S} \tag{4.2}$$

Energy dissipation may be because of soil friction or its non-linear behavior. Even at small strains damping is not zero due to presence of pore water and friction between soil particles. The initial damping before the start of hysteretic loop and hence corresponding damping is given by Rayleigh damping as discussed in previous sections.

The variation of shear modulus, *G*, normalized with small strain maximum shear modulus, G_{max}, plotted against shear strain, γ, is known as modulus reduction curve. In the past, researchers have developed shear modulus and damping variation curves with shear strain in soils. These curves are result of a series of experiments involving resonant column and triaxial shear test to determine lower and higher strain values respectively. The variation of soil properties with shear strain has been observed to be dependent on a number of parameters such as soil density, γ, plasticity index, PI, Poisson's ratio, μ, confining stress, σ_m. Later researchers (Baris Darendeli 2001; Jianfeng et al. 2005; M. Duncan and Chang 1970) have developed equations for normalized shear and damping ratios for quaternary, tertiary and residual soils using modified hyperbolic model given by the equation:

$$\frac{G}{G_{\max}} = \frac{1}{1+\left(\frac{\gamma}{\gamma_{ref}}\right)^{\alpha}} \tag{4.3}$$

Where γ_r is the reference strain, defined as the strain value where G/G_{max} ratio reduces to half and α is a curve fitting parameter.

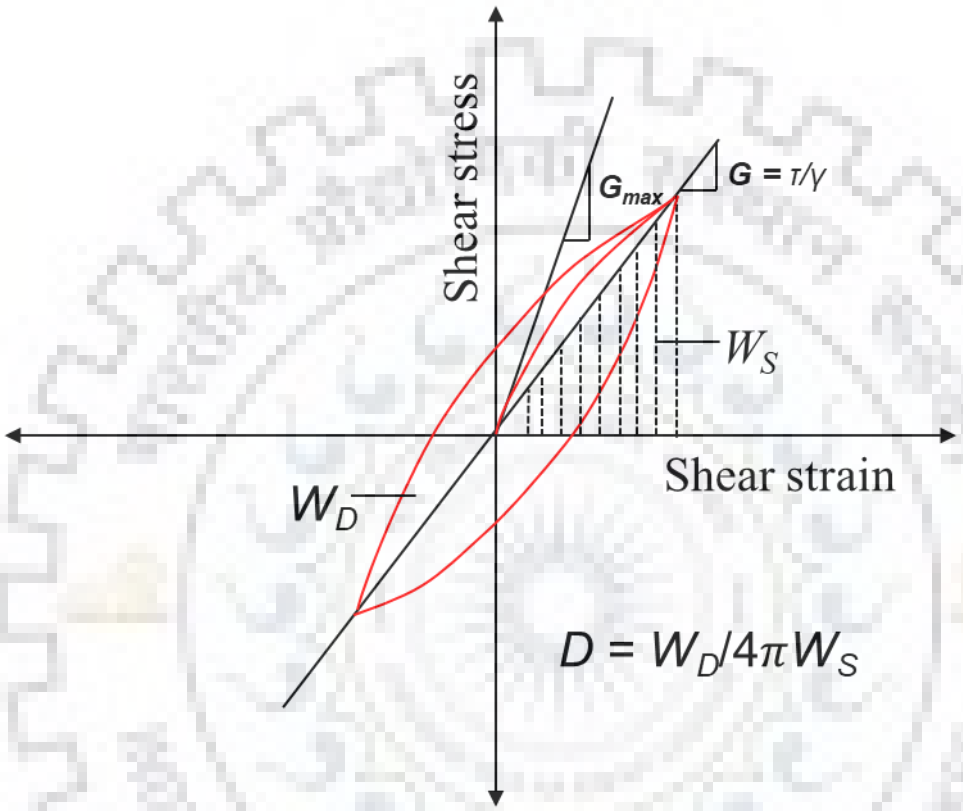

Figure 4.1 Hysteresis loop for one cycle of loading showing G_{max}, G and D.

In the present study the equations developed by Jianfeng (2005) are used to develop shear modulus curves. Different backfill profiles have been taken for the parametric study resting on two foundation profiles C and D discussed earlier. To estimate the initial shear modulus, G_{max}, shear wave velocity for the backfill has been assumed corresponding to C and D category soil type. The variation of shear modulus for different backfills and soil parameters are given in Fig.4.2 and Table 4.1 respectively. Soil parameters have been selected from soil classification given by Unified Soil Classification System (USCS) with non-associated flow rule taking realistic dilation angle values, ψ, (Loukidis et al. 2008). Shear modulus is then calculated using Eq.4.1

Table 4.1 Backfill Soil Parameter.

Parameter	Backfill		
No.	**1**	**2**	**3**
Friction angle, ϕ	30˚	35˚	40˚
Dilation angle, ψ	2˚	6˚	12˚
Density, γ, (kN/m^3)	17	18	19
Poisson's ratio, μ	0.3	0.3	0.3

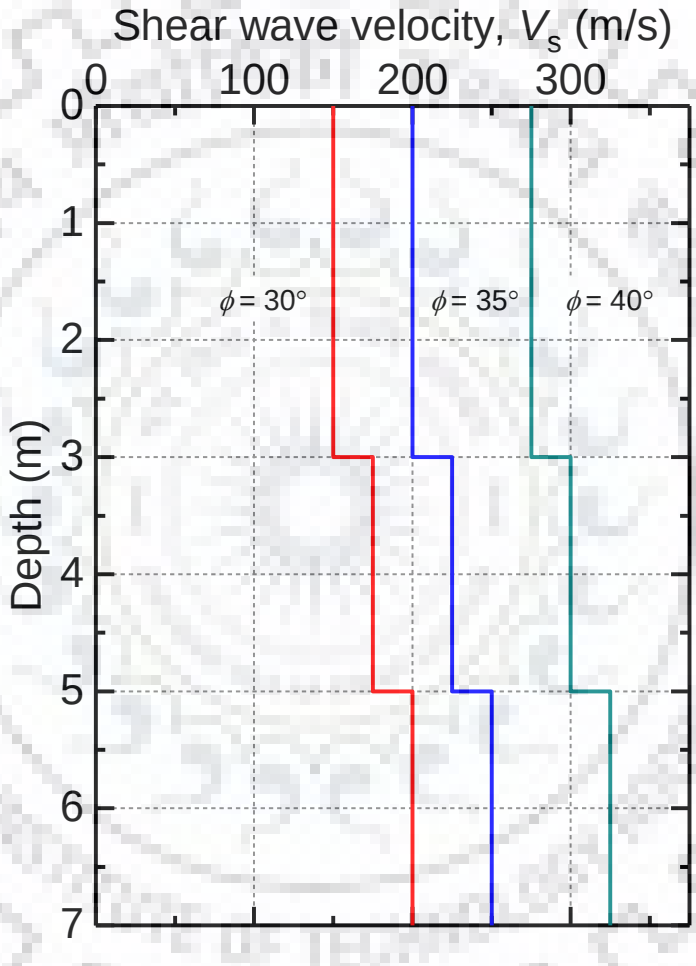

Figure 4.2 Variation of shear wave velocity along depth for different backfills.

Soil non-linearity in the backfill and foundation have been incorporated in the present study through incorporating modulus ratio curves developed by the equations given in the study by Jianfeng (2005). Backfill soil is considered to be in the residual soil classification as in the practical retaining problems the backfill made up of residual soil and foundation soil is taken to be of quaternary type which are older in age in comparison to residual.

As the backfill is considered to be cohesion less, its plasticity index is taken to be zero for all cases. In case of foundation the PI values are computed from the graph between soil friction angle, ϕ, and PI (Bowels 1996) as shown in Fig for soil type C (ϕ = 40^o) and D (ϕ = 36^o) corresponding to undisturbed soil. The modulus reduction curve generated corresponding to PI and confining stress σ at the center of each layer in the backfill and foundation are incorporated in the FE model properties till reference strain, *i.e.* where shear modulus reduces to half of its initial value. The path followed by the stress-strain curve is shown in Fig. 4.4.

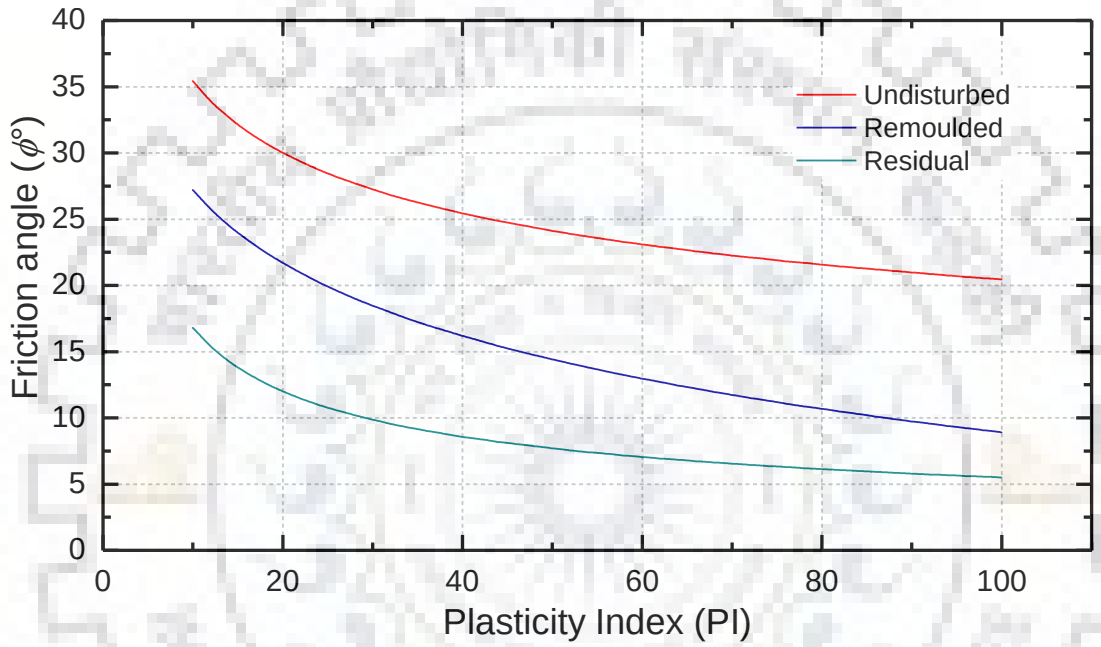

Figure 4.3 Variation of PI with soil friction angle for undisturbed, remoulded and residual soils (Bowels 1996).

Figure 4.4 shows difference between the stress-strain curve with initial stiffness G_{max}, an elasto-plastic model with shear stiffness reduced to 65% and 50%. It also demonstrates the actual non-linear stress-strain curve incorporated in the present study up to reference strain where shear stiffness reduces to 50% of its initial value. Taking the elasto-plastic model with initial stiffness will make the system highly stiff, which reduces its response considerably compared to the actual non-linear behavior. Same problem is faced with an elasto-plastic model with a reduced stiffness of 50% directly. In order to simulate an accurate and computationally easier response of this curvilinear behavior of the system, an approach is followed in which 1D equivalent non-linear system is used to compute the average reduction value of shear modulus in soil layer. In this study approach has been made to simulate the actual non-linear behavior as shown in Fig.4.4.

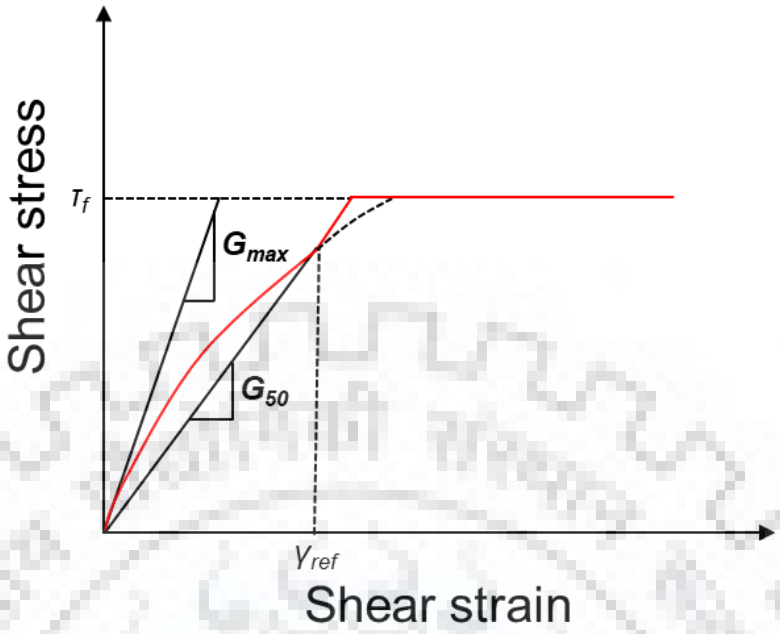

Figure 4.4 Typical stress-strain curve for cohesion-less soil.

4.2 Incremental Dynamic Analysis

Incremental dynamic analysis (IDA) is a time history time history analysis using ground motion suites. The ground motions are normalized to match with the target spectra within the period of interest. The target spectra can be a general response spectrum, site specific spectra or multi-site specific spectra as in Capacity Mean Spectrum approach. The component of ground motion selected is corresponding to maximum of peak ground acceleration value out of the two horizontal motions. Unlike Non-linear time history analysis (NLTHA) the ground motions are scaled from elastic to complete collapse range. This helps in studying the systems response with increase in demand in a better way.

The suite of ground motions normalized with the target spectra is recorded at rock outcrop. In order to directly apply the ground motions in the model, they need to be de-convoluted up to the depth of rock bed. This can be done using software which have formulation to de-convolute for example DEEPSOIL, SHAKE 2000. The ground motions de-convoluted to a depth of 57 m to the rock base are applied as an acceleration field at the base of the finite element model. The ground wave propagation is assumed to be vertical. The response of the system for all ground motion scaled from elastic to plastic region is computed and plotted against the intensity measure, a parameter to quantify

demand, and a corresponding mean value is estimated. This process helps in estimating the uncertainties associated with the demand, $\beta_{d.}$ The uncertainties associated with capacity and definition of damage states is specific to the system under consideration. A common value for these uncertainties in case of abutment is taken as $\beta_{ds} = 0.4$, $\beta_c = 0.3$ (Argyroudis et al. 2013; Pitilakis et al. 2014b; Raj 2018) for uncertainty in definition of damage state and uncertainty due to response of model respectively.

The definition of the damage states plays an important role in the total uncertainty β_{tot}. The limit of the system's response exceeding a particular damage state is decided by the expert's judgement. Then a cumulative log-normal distribution is plotted to quantify the probability of exceedance for a particular damage state with the imposed demand also known as fragility curves (Pitilakis et al. 2014b).

4.2.1 Damping

In ABAQUS, damping needs to be modelled as frequency dependent Rayleigh damping which is defined by two parameters α and β which can be given by equations 4.4 and 4.5:

$$\alpha = \frac{2\omega_i\omega_j}{\omega_i + \omega_j}\xi \tag{4.4}$$

$$\beta = \frac{2}{\omega_i + \omega_j}\xi \tag{4.5}$$

where, ξ = damping ratio, ω_i and ω_j corresponds to the frequencies having damping exactly equal to damping ratio and at other frequencies damping varies with the equation 4.6:

$$\xi_k = \frac{\alpha}{2\omega_k} + \frac{\beta\omega_k}{2} \tag{4.6}$$

ξ_k can be obtained using corresponding values of $\omega_{k..}$ Plot of the above equations shows that damping for the frequencies in between ω_i and ω_j will have less damping than the mentioned damping ratio and for the frequencies lie outside ω_i and ω_j will have higher damping ratio. So, wider range of ω_i and ω_j will give flatter curve for in between frequencies.

4.2.2 Selection of Ground Motions

The selection of the ground motion for the study depends on the spectral matching of their average with the target spectra. Code ASCE/SE17-16 (2017) recommends a minimum of 7 ground motions or a suite of 11 or more ground motions. Thus a suite of 11 ground motions time histories of real earthquakes is used in this study using PEER database (https://ngawest2.berkley.edu/). The ground motions selected have shear wave velocity Vs>600 m/s and epicentral distance less than 10 km. The time histories were frequency filtered and baseline corrected to ensure proper wave propagation without any distortion while propagating through the system. Fig.4.5 below shows the spectra of all selected ground motions compared with the target spectra.

It can be seen that the selected suite spectra are in good agreement with the target spectra. The ground motions are than de-convoluted in DEEPSOIL software to a bedrock depth of 60 m and applied at the bedrock level. The details of the selected time histories are given in Table 4.2

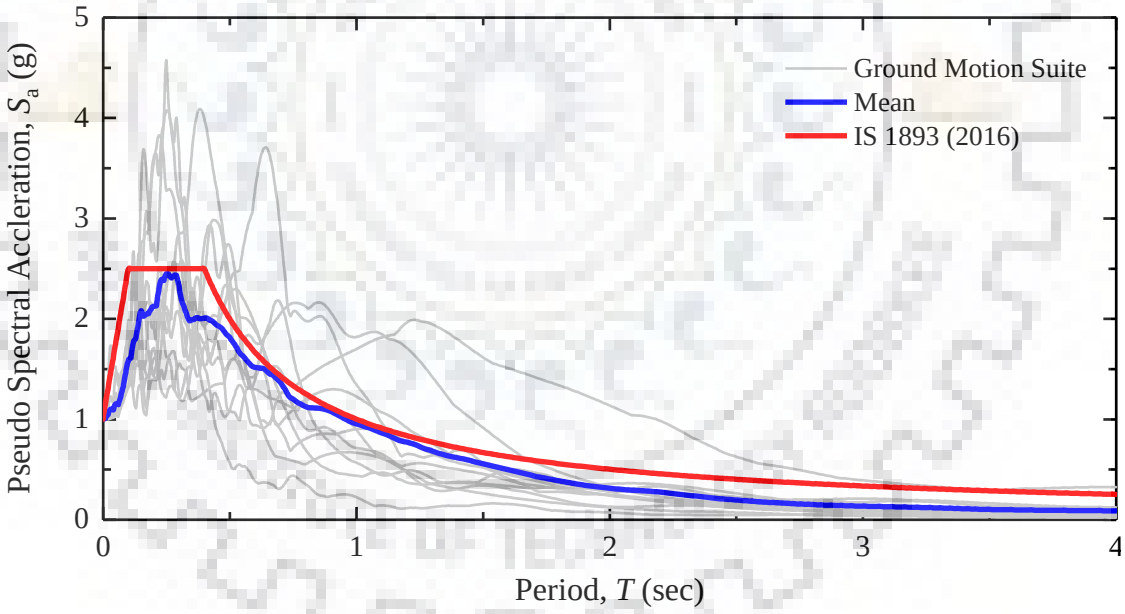

Figure 4.5 Comparison of the selected ground motion spectra with the design spectrum of IS1893 (2016).

Generally, 5% damped first mode spectral acceleration is used as Intensity measure parameter for IDA. But for a coupled system adopting $S_a(T_1)$ is not appropriate as IM. So a more reliable parameter would be Peak ground acceleration recorded at rock outcrop. Although the variability in response using other IMs is less as compared to peak ground acceleration but for a coupled system there is an increase in time period due to

soil-structure interaction. This makes dependency of systems' response unreliable using fundamental time period. Thus Peak ground acceleration (PGA) is used as IM in the present work. This simplifies the uncertainties and makes comparison easier with available fragility curves.

4.3 Validation of Stress-Strain Model of Soil

Incorporation of actual non-linear stress strain profile is difficult in the finite element system. In order to account for soil behavior, a simpler approach of 1D equivalent linear ground response analysis is considered. In this approach a calibration process is followed and an average reduction coefficient is determined corresponding to the strain generated in the soil profile for different dynamic loading. The reduction through this calibration process depends on the soil type. However, it generally varies in between 0.6-0.7 times the initial stiffness.

The following section compares horizontal displacement of the wall and vertical displacement of the backfill obtained from the methodology, shear modulus as a function of shear strain, G_γ, used in present study with the direct reduction of 50% in the initial stiffness for two different earthquakes. A comparison has also been made with a reduction of 0.6, 0.65 with the present study methodology.

As can be observed from the comparison of the results obtained through direct reduction in shear modulus and the methodology used in the present study, there is a close agreement between them for a direct reduction of 60-70%.

Table 4.2 Details of Selected Ground Motion Suite.

Earthquake	**Year**	**Station**	**Moment Magnitude, M_w**	**PGA (g)**	**R_{jb} (km)**	**Arias Intensity (m/sec)**	**Mechanism**	**V_{s30} (m/sec)**
Chi-Chi, Taiwan	1999	TCU071	7.62	0.65	0	9.5	Reverse oblique	624.85
Duzce, Turkey	1999	Lamont 531	7.14	0.16	8.03	0.4	Strike slip	638.39
Loma Prieta	1989	Gilroy - Gavilan Coll.	6.93	0.36	9.19	0.9	Reverse oblique	729.65
Irpinia, Italy-01	1980	Bagnoli Irpinio	6.9	0.19	8.14	0.4	Normal	649.67
Kobe, Japan	1995	Kobe University	6.9	0.31	0.9	1.2	Strike slip	1043.00
Tottori, Japan	2000	SMN015	6.61	0.274	9.1	0.4	Strike slip	615.55
Nahanni, Canada	1985	Site 1	6.76	1.20	2.48	3.9	Reverse	605.04
Northridge-01	1994	LA - Chalon Rd	6.69	0.22	9.87	0.7	Reverse	740.05
San Fernando	1971	Pacoima Dam (upper left abut)	6.61	1.24	0	8.9	Reverse	2016.13
L'Aquila, Italy	2009	L'Aquila - V. Aterno -Colle Grilli	6.3	0.52	0	1.4	Normal	685.00
Morgan Hill	1984	Gilroy Array #6	6.19	0.32	9.85	0.9	Strike slip	663.31

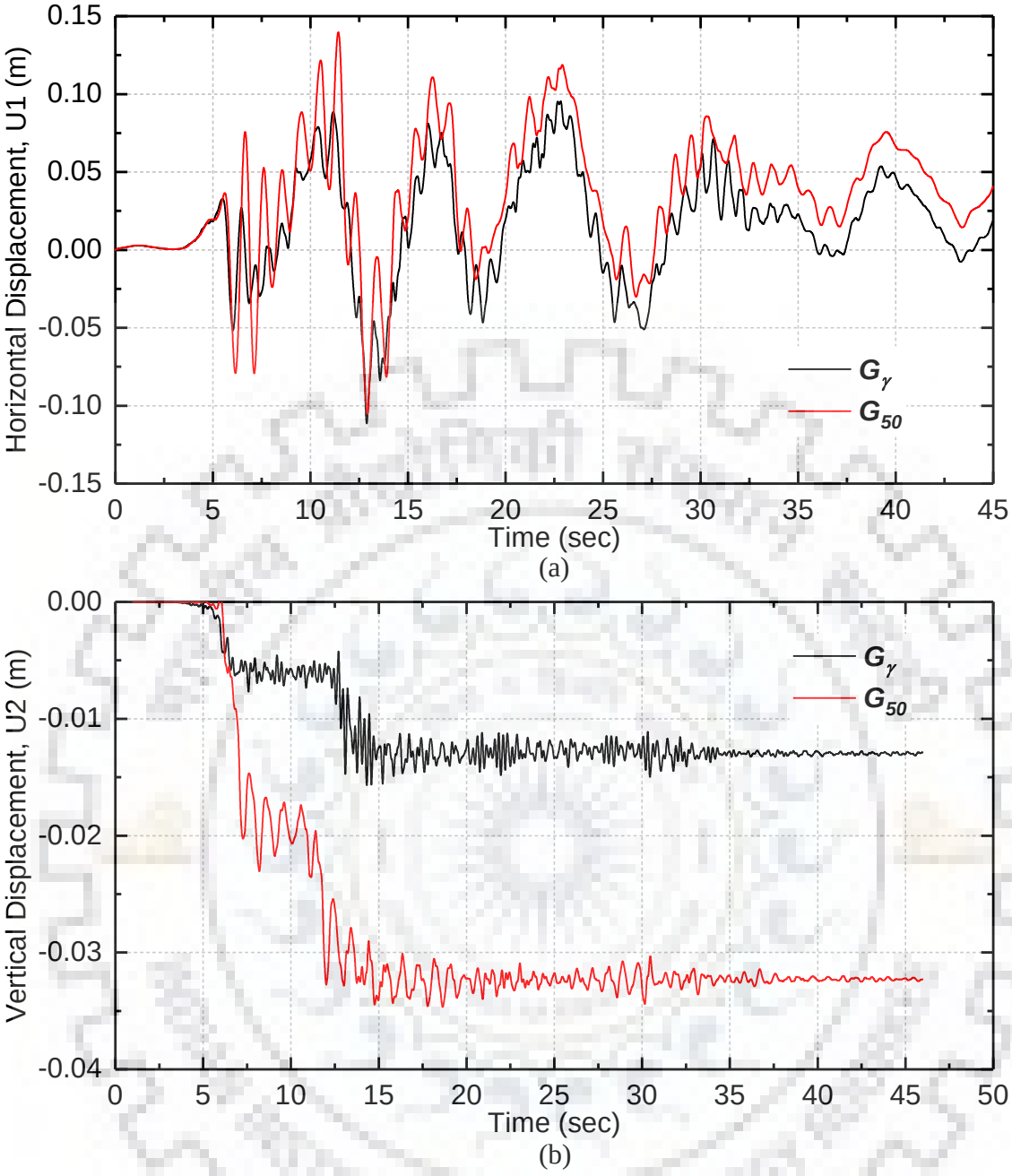

Figure 4.6 Comparison of response obtained using a realistic non-linear stress-strain model and an elasto-plastic model with initial modulus reduced to 50% (Chi-Chi Earthquake, PGA= 0.2g) in terms of (a) horizontal displacement, U1; and (b) vertical displacement, U2.

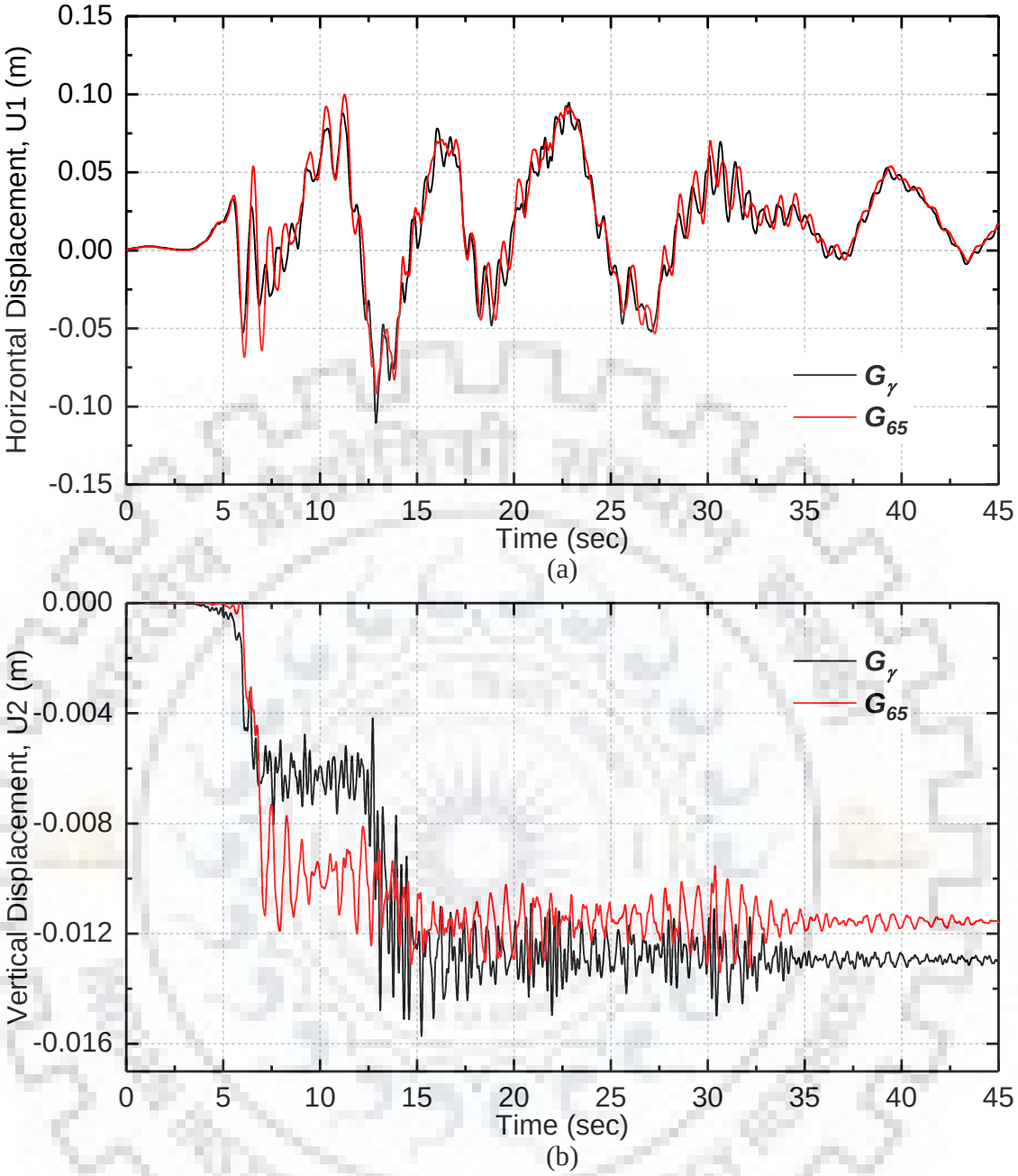

Figure 4.7 Comparison of response obtained using a realistic non-linear stress-strain model and an elasto-plastic model with initial modulus reduced to 65% (Chi-Chi Earthquake, PGA= 0.2g) in terms of (a) horizontal displacement, U1; and (b) vertical displacement, U2.

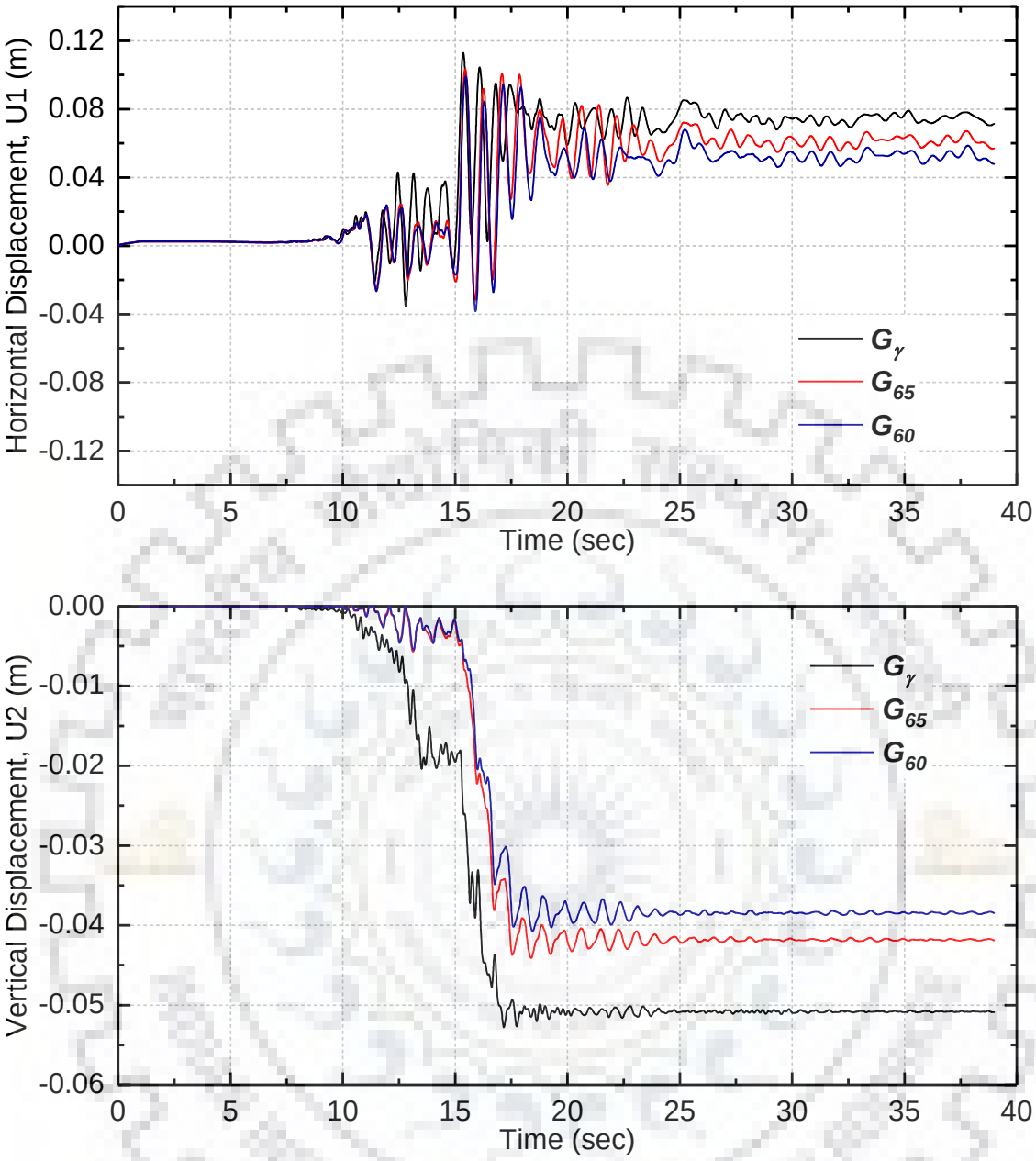

Figure 4.8 Comparison of response obtained using a realistic non-linear stress-strain model and an elasto-plastic model with initial modulus reduced to 60% and 65% (Nanhanni Earthquake, PGA= 0.3g) in terms of (a) horizontal displacement, U1; and (b) vertical displacement, U2.

Chapter 5 Fragility Analysis

5.1 Introduction

Seismic risk assessment is a means of estimating the probability of damage due to seismic forces. Majority of real field problems require the availability of some method to quantify the risk for the estimation of potential loss and damage involved. The vulnerability or fragility functions are used as an approach to describe the vulnerability of structures.

Vulnerability can be defined as the probability of losses which can be social or economic whereas fragility gives the probability of exceeding different limit states for a level of ground shaking. The vulnerability functions can be derived from the fragility functions with the help of consequence functions describing the probability of loss. Fragility curves are expressed in terms of lognormal distribution function (Eq. 5.1) as:

$$P_f\left(ds \geq ds_i \mid IM\right) = \Phi\left[\frac{1}{\beta_{tot}} \ln\left(\frac{IM}{IM_{mi}}\right)\right] \tag{5.1}$$

$P_f(.)$ denotes probability of being or exceeding a damage state, *ds* is the damage state generally determined through expert opinion, *IM* is the intensity measure representing the seismic intensity level of earthquake through PGA, PGV, PGD, ϕ is the standard cumulative probability function, IM_{mi} is the median threshold value to cause any particular damage state, β_{tot} is the log-normal standard deviation.

Fragility curves are crucial in the seismic risk assessment by relating the seismic intensity with the probability of exceeding a damage state (minor, moderate, extensive, collapse) for the element in consideration with increase in the seismic intensity. In the past researchers have developed fragility curves for probabilistic estimation of loss and risk assessment for structures like low and high rise buildings, bridges, tunnels, embankments and retaining structures (Argyroudis et al. 2013, 2016; Argyroudis and Kaynia 2015; Sotiris et al. 2019; Zamiran and Osouli 2018a).Seismic intensity can be defined in terms of peak ground acceleration (PGA), peak ground displacement (PGD), peak ground velocity (PGV) or through spectral acceleration/velocity/displacement.

5.2 Methodologies of Fragility Analysis

Different methods, including empirical, analytical, expert elicitation and hybrid. are used to derive fragility function for estimation of risk associated with a seismic hazard intensity. Analytical methods along with their validation through experimental data are being used in the recent years due to availability of better computational tools which allows parametric studies covering all possible uncertainties like in material properties, ground motion etc. This helps in rigorous non-linear time history and incremental dynamic analysis.

5.2.1 Empirical Methods

Empirical approach involves study of past earthquakes data and field surveys of damage caused to elements under consideration. This gives an idea about the various damage states limits under earthquake loadings. As empirical curves are derived from field data, they account for the variability in the structure type, field condition interaction with the structure and the failure mechanism. However empirically derived fragility curves have disadvantage of being associated with a particular site field data and intensity of certain recorded earthquakes only. This considerably reduces their dependability and robustness and imparts uncertainty to the analysis. The limited availability and its dependability on the earthquake damage data makes its use even less trustworthy.

5.2.2 Expert Judgement

This approach entirely depends on judgement and experience of the appointed experts estimating the loss and the risk for different intensities. Analysis method includes vulnerability assessment through visual diagnostics of the structure after a seismic event. The advantage of being independent of the lack of extensive damage data (empirical) and no reliability of the result on the structural models (analytical). The major problem with this approach is its dependence on an individual expertise. Although this bias in curves can be reduced with increasing the number of experts their use is restricted in different countries due to different engineering practices.

5.2.3 Analytical Methods

In analytical approach the structures' response to a seismic input is used to estimate damage. The input methods can be static (response spectrum) and dynamic (NLTHA).

For analysis numerical models are developed to simulate the actual behavior of the structure. Analytical methods used for analysis are Capacity Spectrum Method (CSM) and Incremental Dynamic Analysis (IDA).

5.2.3.1 Capacity Spectrum Method

Structures are in general categorized by a bilinear capacity curve developed for an equivalent single degree of freedom system which involves static pushover analysis. These curves are converted to spectral acceleration-displacement and plotted with the response spectrum to obtain the performance point of an element which is the spectral displacement corresponding to a particular damage state.

5.2.3.2 Incremental Dynamic Analysis

In incremental dynamic analysis (IDA), a suite of ground motion is used to perform non-linear time history analysis. The ground motions are scaled to cover the range from elastic to complete collapse of the structure. The scaling of ground motions gives a good estimate of the response of the structure to seismic loading also known as engineering demand parameter (EDP). The demand parameter generally used in case of abutment is the backfill vertical settlement or displacement of the abutment top relative to free-field condition which might cause its failure during an earthquake.

5.2.4 Hybrid Methods

A hybrid method is the combination of methods like empirical and experimental methods. This helps in overcoming the disadvantages of one method over other and combining their advantages. For example, analytical methods require defining the damage states such as minor, moderate and extensive. These damage states are defined on the basis of expert judgement and their experience.

5.3 Damage States

Limit states represents the performance level of a structure subjected to a seismic intensity and defines the boundary of a particular damage condition referred to as damage states. These damage states represent the functionality and serviceability level of components. The definition and selection of the damage states is one of the main sources of uncertainties in the fragility analysis of a structure. The damage states' definition is usually based on experts' judgment. The damage states limits used in the present study

are based on experimental observations and damage state definitions used in previous studies (Huang et al. 2009; Yingwei and Shamsher 2019; Zamiran and Osouli 2018b). These damage states form four zones defining damage level as minor, moderate, extensive and collapse. Description of these damage states is given in Table 5.1:

Table 5.1 Definition of Damage States.

Description of Damage States	Damage States' Limit	Normalized displacement value (H = 6m)
Permissible or minor damage (DS_1)	0.02H or 2%	0.12
Moderate damage (DS_2)	0.05H or 5%	0.3
Complete collapse (DS_3)	0.08H or 8%	0.48

5.4 Intensity Measures

Intensity measure (IM) of an earthquake is representative of its strength characteristics and also defines the response of the element. Thus the selection of an IM depends on the extent to which it represents the damage to the systems. IMs are categorized as: empirical and instrumental intensity measures. Empirical IMs uses macroscopic intensity scales to represent the effect of a ground motion. Instrumental IMs on the other hand uses an analytical value to represent the severity of a seismic event recorded.

5.5 Uncertainties

Uncertainties in the risk assessment might originate from the derivation methodology, parameters, and definition of damage states in fragility curves. Uncertainties can be classified as aleatory and epistemic uncertainties. The aleatory uncertainties represent the intrinsic randomness whereas epistemic uncertainty is due to lack of available data and knowledge about a phenomenon.

The uncertainty in fragility analysis is defined through standard deviation, β_{tot}, which consists of uncertainty due to 3 different parameters: β_{ds}, due to uncertainty in definition of damage states, β_c, due to response of the model and βd, due to variability in input ground motion due to different frequency content, epicentral distance. Improper

definition and lack of knowledge of threshold of damage state results in β_{ds}. Uncertainty due to capacity occurs due to the error in modelling and the variability of a ground motion in terms of their radial distance, depth, magnitude etc. The total variability is found assuming independent and lognormal distribution of the contributors as:

$$\beta_{tot} = \sqrt{\beta_{DS}^2 + \beta_C^2 + \beta_D^2} \tag{5.2}$$

The uncertainty in definition of damage states and response of the system are selected depending on the system under consideration. In the present study to estimate the response of abutment-backfill system the uncertainty factors are taken as 0.4 and 0.3 for uncertainty in definition of damage states, β_{ds}, and modelling, β_c. The uncertainty due to variability in ground motions is estimated through time history analysis with 11 ground motions as recommended ASCE/SE17-16 (2017). A pictorial representation of the methodology of estimation of seismic vulnerability is shown in Fig.5.2.

5.6 Median Threshold Value

Median threshold (IM_{mi}), is the value required to cause a particular damage state. Figure 5.1 shows different points of the response of the system known as damage index plotted against the intensity measure. A regression analysis is performed to obtain the solid line and the IM_{mi} value is obtain by the definition of the damage states through damage index.

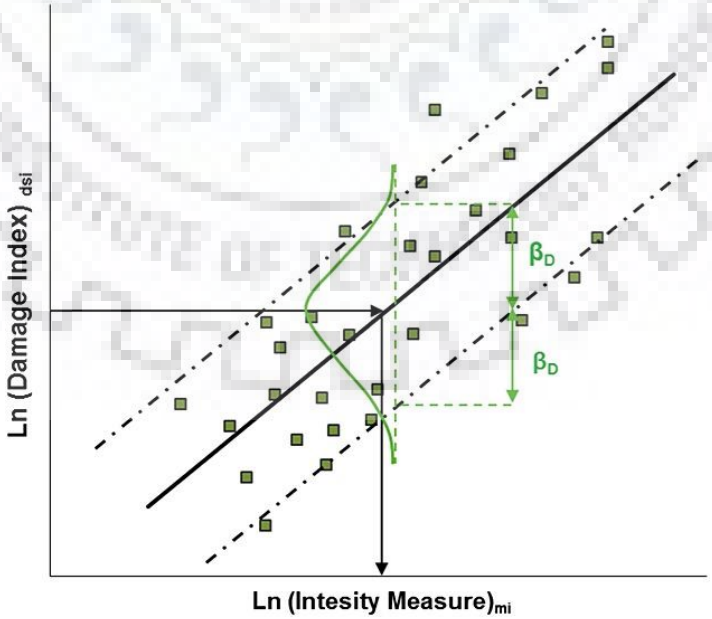

Figure 5.1 Example of evolution of damage with earthquake *IM*, IM_{mi} for a damage state and β_D due to variability of input motions (Argyroudis and Kaynia 2015).

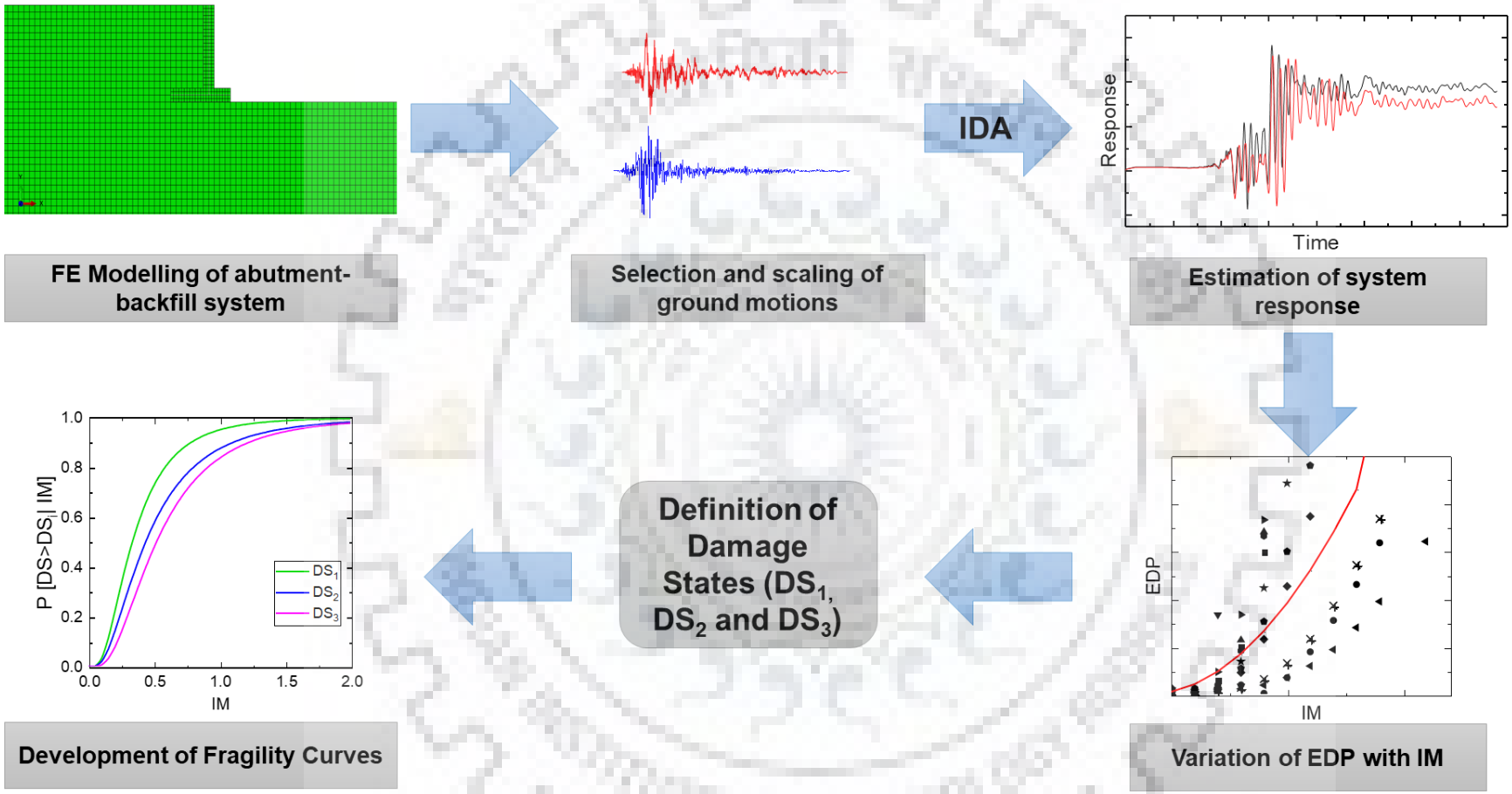

Figure 5.2 Methodology for estimation of seismic vulnerability of abutments. (Raj 2018).

5.7 Results and Discussion

Incremental Dynamic Analysis performed through a 2D non-linear model prepared in ABAQUS was used in the present study to get the response of the abutment-backfill system during a seismic event. The details of the ground motions, their selection procedure and progressive scaling procedure has been discussed in the previous chapter. The results of the IDA have been examined at the top of the abutment in terms of maximum horizontal displacement, $U_{h,\ Residual}$. Residual displacement of abutment is defined as the displacement of the top of abutment relative to free field condition.

The distribution of shear force and bending moment is required for design of any structure. An attempt has been made to get a distribution of the forces during a seismic event. The results of IDA for different foundation with varying peak ground acceleration, have been used, in order to generate envelopes of the maximum shear force and bending moment, as shown in Figs. 5.4 and 5.5. In order to highlight the effect of bridge superstructure mass acting at the top of abutment (which is the difference between a problem of retaining wall and an abutment) a separate analysis was performed without taking the inertial mass of superstructure (taken 200kN) in the present study. Fig. 5.3 shows the difference between the bending moment and shear force distributions in the two cases.

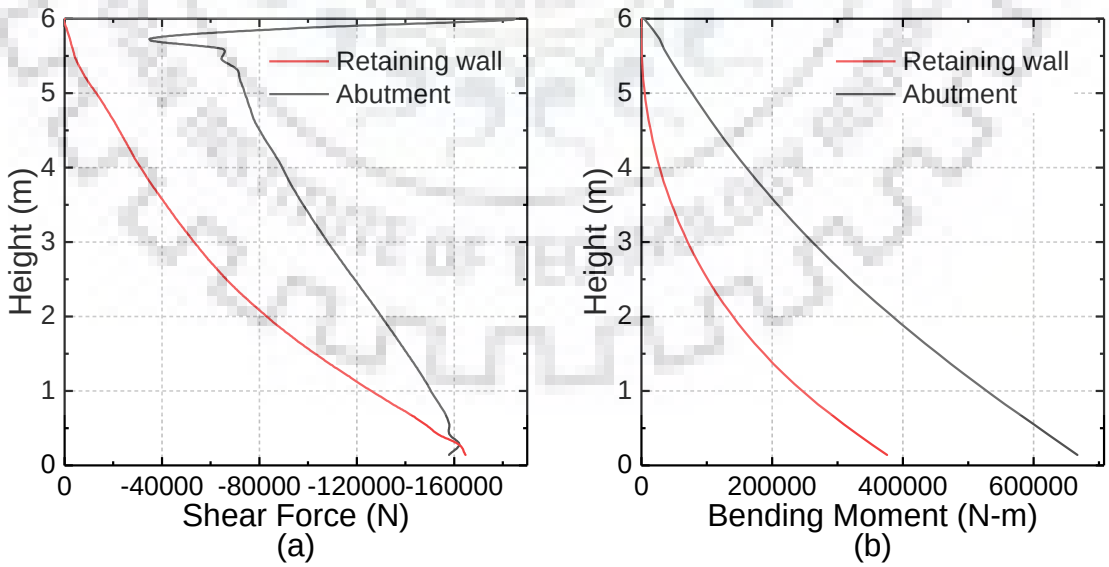

Figure 5.3 Effect of superstructure mass on top of a bridge abutment, on the abutment forces, in comparison with a retaining wall having identical conditions: (a) shear Force; and (b) bending moment.

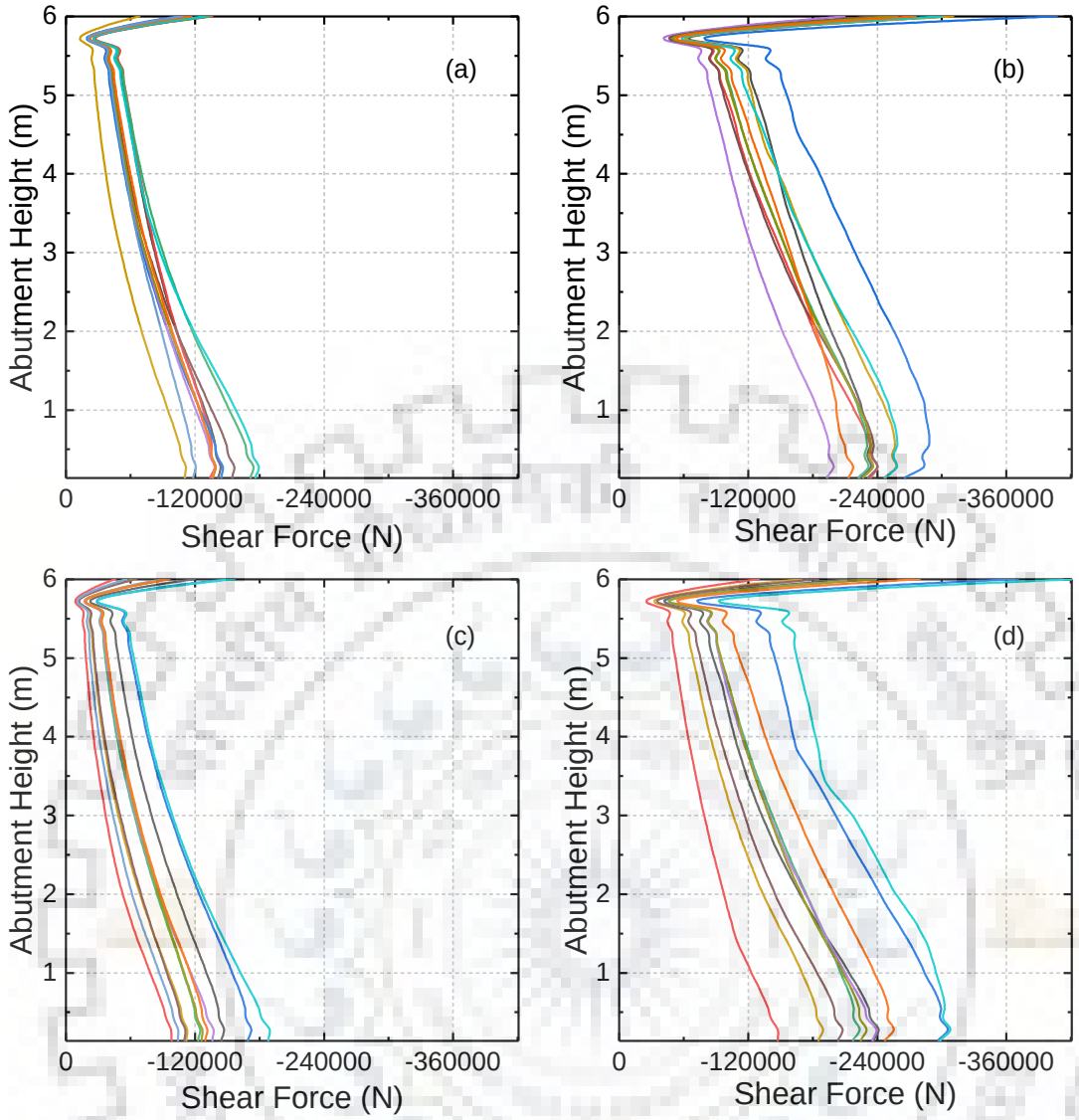

Figure 5.4 Shear force envelops for: (a) ground motions with PGA scaled to 0.1g on foundation Type – C; (b) ground motions with PGA scaled to 0.3g on foundation Type – C; (c) ground motions with PGA scaled to 0.1g on foundation Type – D; and (d) ground motions with PGA scaled to 0.3g on foundation Type – D.

The bending moment at the base of the abutment when compared with the case of retaining wall (Fig. 5.3(b)) shows a large variation at the base. This is due to the participation of dead load of the superstructure in a seismic event. The distribution of the shear force and bending moment acting on the abutment during a seismic event is as shown in Fig. 5.4 and 5.5 respectively.

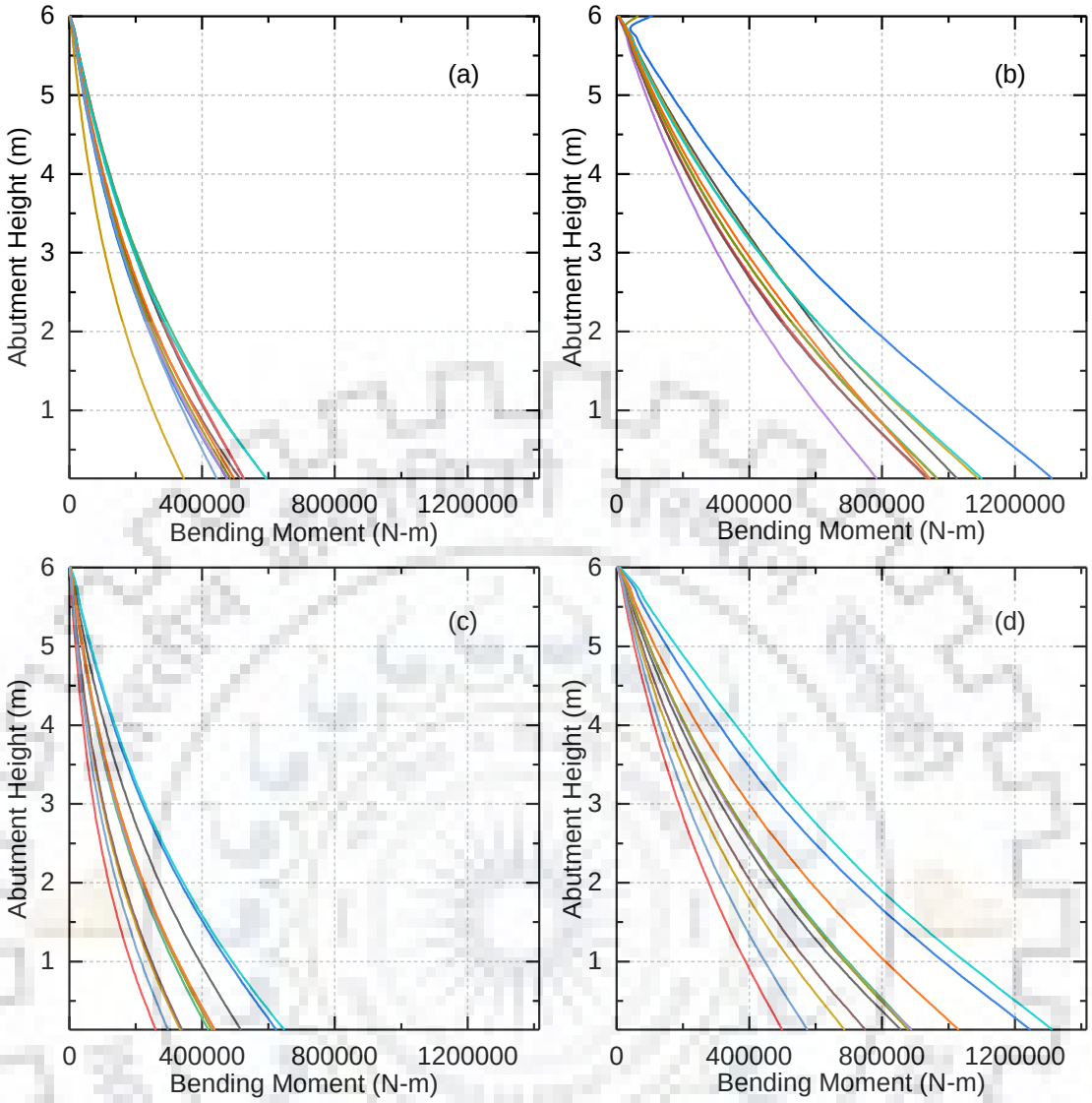

Figure 5.5 Bending moment envelops for: (a) ground motions with PGA scaled to 0.1g on foundation Type – C; (b) ground motions with PGA scaled to 0.3g on foundation Type – C; (c) ground motions with PGA scaled to 0.1g on foundation Type – D; and (d) ground motions with PGA scaled to 0.3g on foundation Type – D.

The response of the system in terms of horizontal displacement at the top of abutment is shown with increasing peak ground acceleration (PGA) in Fig 5.6. The following observations can be made from the response:

1. The peak ground acceleration to cause minor damage (DS_1 - 0.12 m), moderate damage (DS_2 - 0.3 m) and collapse damage (DS_1 - 0.48 m) increases for both the foundations (Type C and D), with increase in backfill friction angle, ϕ, and density, γ.
2. The response of the abutment also depends on the foundation underneath. It is interesting to note that although shear modulus, cohesion, density, friction angle and

other soil parameters are higher for Foundation Soil Type C than Type D, abutment reaches collapse state at a smaller PGA for foundation Type C than Type D. The possibility of natural frequency of Type C close to forcing frequency of the ground motions might be a reason in amplification of its response.

3. A large variation in the systems' response can be observed corresponding to different ground motions. This variation is attributed to a wide range of forcing frequencies of the ground motions.
4. A weaving nature is observed in the dynamic capacity curve with increasing PGA values for some ground motions. This may be due to change in the frequency of the ground motion at the level of the abutment foundation due to nonlinearity of foundation soil and change in the frequency of vibration of abutment itself due to nonlinearity of the backfill material.

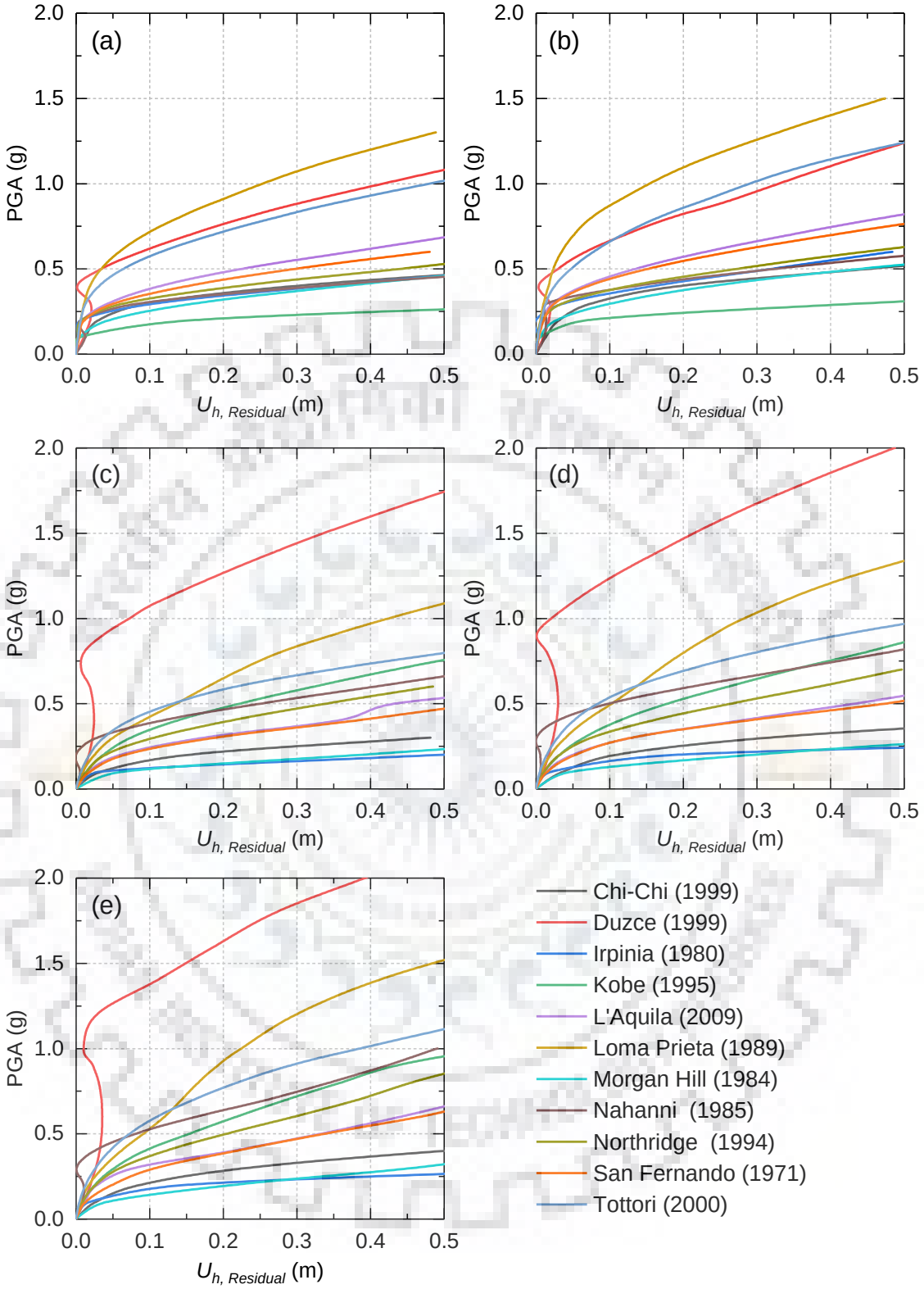

Figure 5.6 Residual horizontal displacement, $U_{h,\ Residual}$, of abutment top with ground motion intensity (represented by PGA) for: (a) abutment with backfill-1 ($\phi = 30^{\circ}$) resting on foundation Type – C; (b) abutment with backfill-2 ($\phi = 35^{\circ}$) resting on foundation Type – C; (c) abutment with backfill-1 ($\phi = 30^{\circ}$) resting on foundation Type – D; (d) abutment with backfill-2 ($\phi = 35^{\circ}$) resting on foundation Type – D; and (e) abutment with backfill-3 ($\phi = 40^{\circ}$) resting on foundation Type – D.

5.7.1 Seismic Fragility of Abutment-Backfill System

Cumulative log-normal distribution functions (CDF) have been used to develop fragility functions and estimate damage probability. It provides a simplified means for seismic risk modelling. A lognormal CDF is a representation of data with upper and lower bound limit of 1 and 0 as is the limit for probability distribution of damage. The lower bound of 0 satisfies the requirement of a non-zero IM and a corresponding probability of 0. Moreover, lognormal distribution when multiplied with a constant result in a lognormal distribution which might be a case in factor of safety for instance.

As described in section 5.6 above, to develop the fragility curves and estimate the uncertainty in demand, β_D, the median values have been determined using regression analysis of the IDA results considering the lognormal distribution of PGA corresponding to damage states limit. Variation of $U_{h,\,Residual}$ for different backfill resting on different foundation types has been shown in Fig.5.7 with increase in PGA. The value of β_{DS} and β_C has been taken as 0.4 and 0.3 based on previous studies (Argyroudis et al. 2013; Pitilakis et al. 2014b; Raj 2018). The estimated parameters have been shown in Table 5.2 and the corresponding fragility curves developed for different backfill-foundation combination have been presented in Fig.5.8.

Table 5.2 Parameters of Fragility Functions for Different Damage States.

Foundation Soil Type	Backfill	DS_1		DS_2		DS_3	
		β_D	β_{tot}	β_D	β_{tot}	β_D	β_{tot}
C	$1(\phi = 30^{\circ})$	0.53	0.66	0.56	0.72	0.57	0.67
	$2(\phi = 35^{\circ})$	0.54	0.65	0.58	0.73	0.62	0.69
D	$1(\phi = 30^{\circ})$	0.57	0.83	0.62	0.97	0.66	0.83
	$2(\phi = 35^{\circ})$	0.59	0.83	0.66	0.95	0.72	0.83
	$3(\phi = 40^{\circ})$	0.61	0.82	0.69	0.96	0.75	0.82

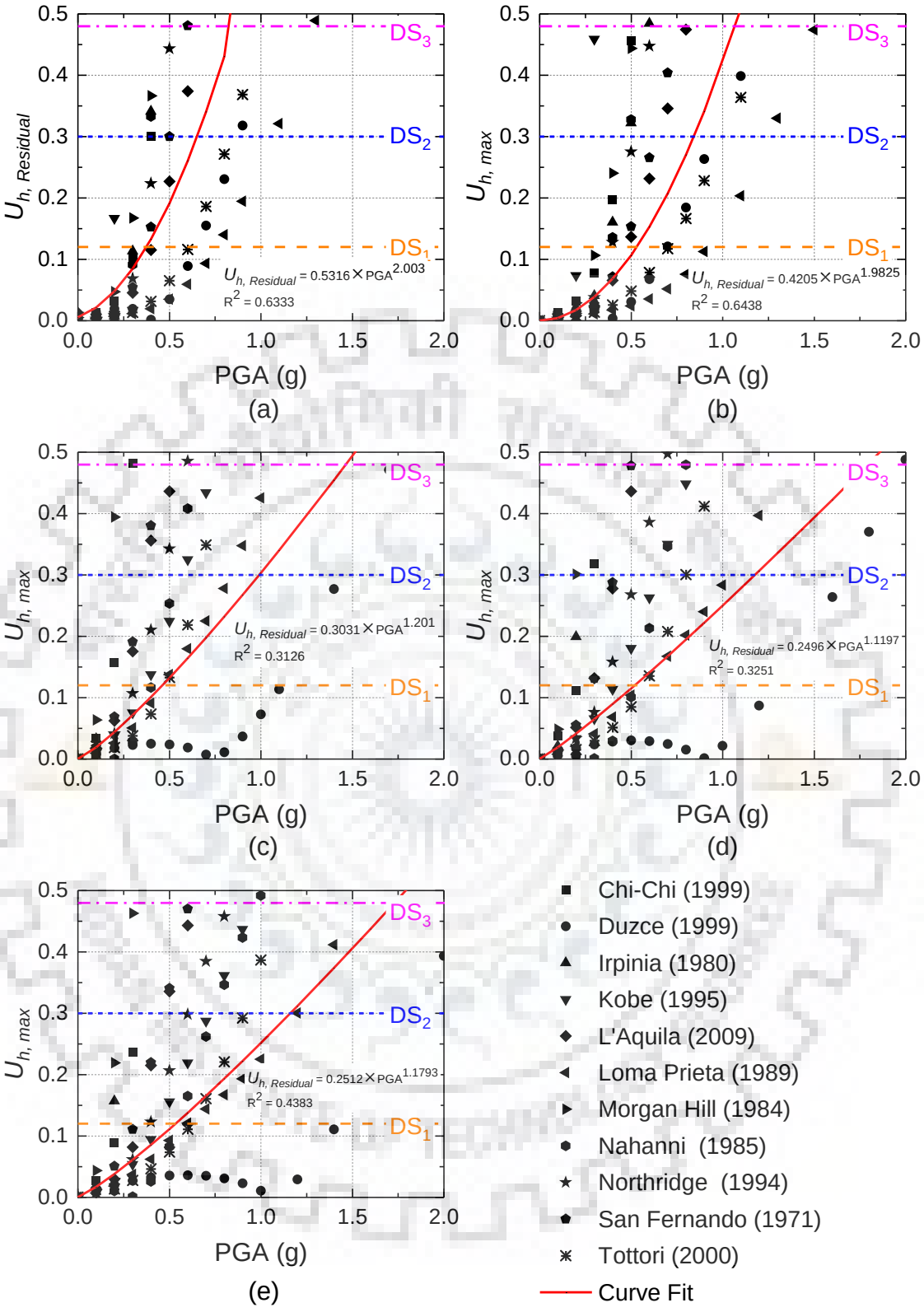

Figure 5.7 Variation of residual horizontal displacement $U_{h,\,Residual}$ of abutment top with increasing PGA for: (a) abutment with backfill-1 ($\phi = 30^{\circ}$) resting on foundation Type – C; (b) abutment with backfill-2 ($\phi = 35^{\circ}$) resting on foundation Type – C; (c) abutment with backfill-1 ($\phi = 30^{\circ}$) resting on foundation Type – D; (d) abutment with backfill-2 ($\phi = 35^{\circ}$) resting on foundation Type – D; and (e) abutment with backfill-3 ($\phi = 40^{\circ}$) resting on foundation Type – D.

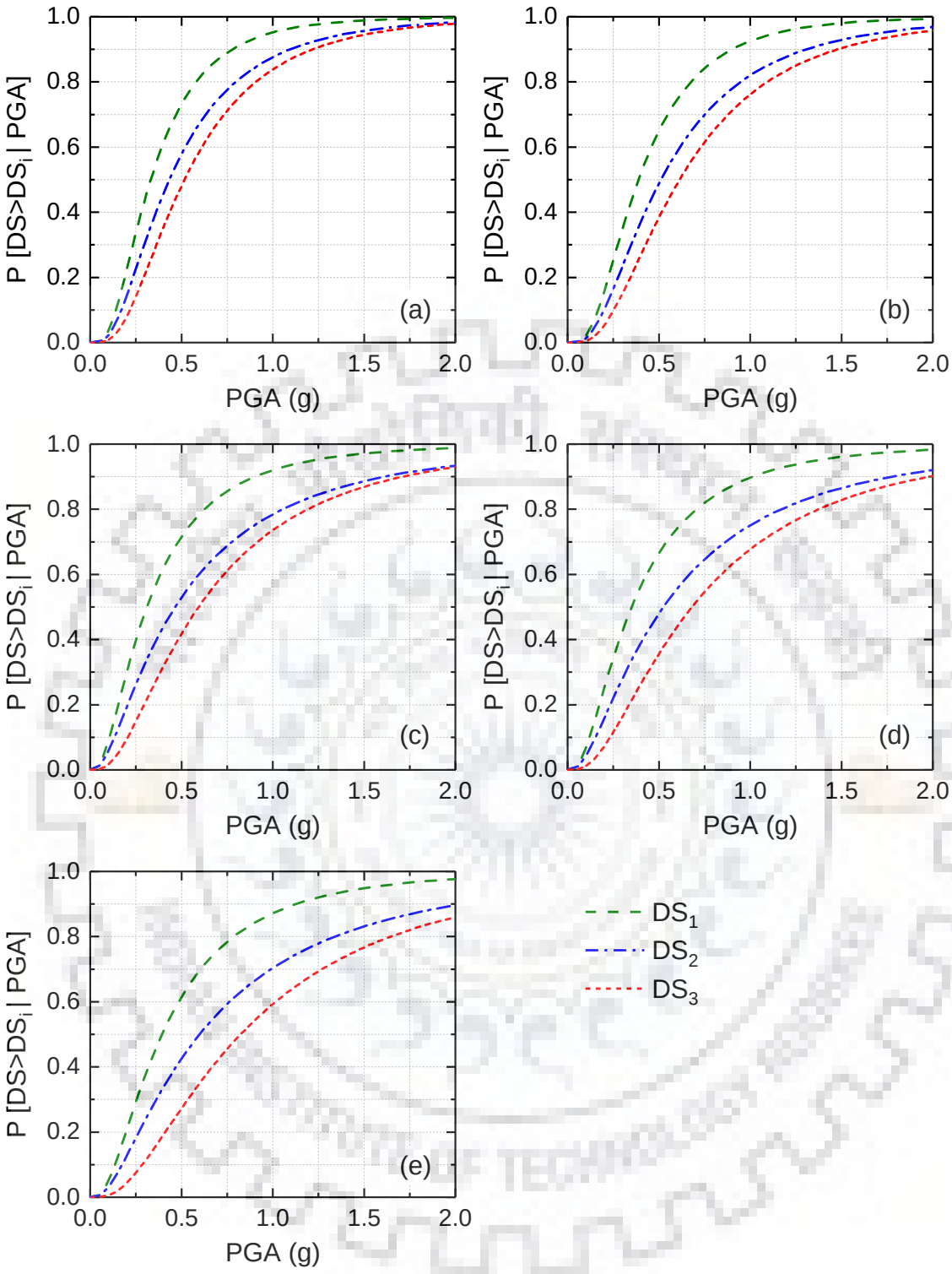

Figure 5.8 Fragility curves for: (a) abutment with backfill-1 (ϕ = 30˚) resting on foundation Type – C; (b) abutment with backfill-2 (ϕ = 35˚) resting on foundation Type – C; (c) abutment with backfill-1 (ϕ = 30˚) resting on foundation Type – D; (d) abutment with backfill-2 (ϕ = 35˚) resting on foundation Type – D; and (e) abutment with backfill-3 (ϕ = 40˚) resting on foundation Type – D.

The comparison of fragility of abutment retaining different backfills and supported on foundation soil Type C and Type D is shown in Fig. 5.9. It can be observed from the cumulative distribution that the probability of minor, moderate and collapse damage states reduces with increase in soil friction angle, ϕ, and density, γ. Although the reduction in collapse state probability is not as significant as in case of the other two damage states.

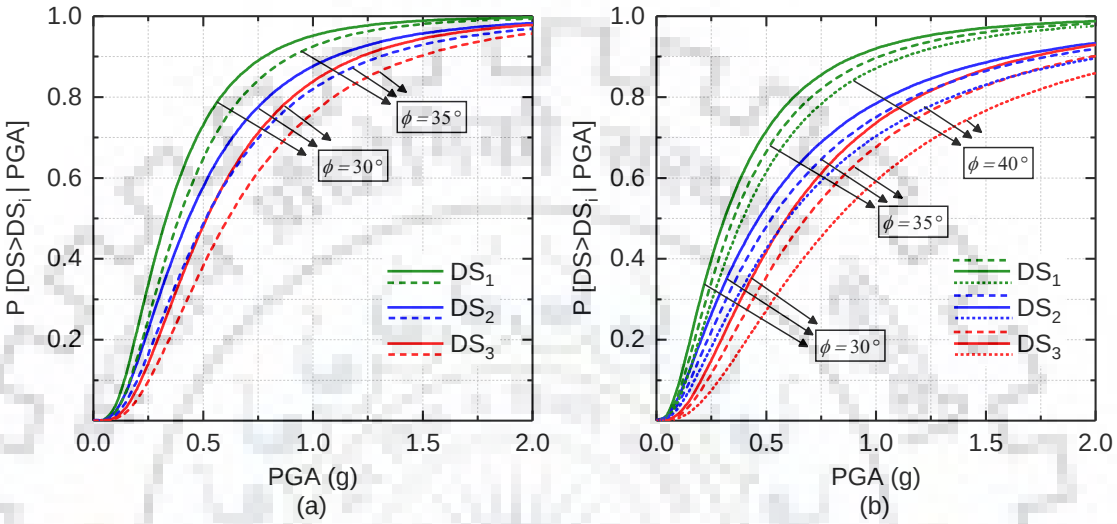

Figure 5.9 Comparison of fragility curves for abutments with different backfills and resting on foundation: (a) Type – C; and (b) Type – D.

Table 5.3 Probability of Different Damage States (%) for Different Seismic Zones.

Foundation Soil Type	Backfill	DS$_1$				DS$_2$				DS$_3$			
		II	III	IV	V	II	III	IV	V	II	III	IV	V
C	1($\phi = 30°$)	4	13	31	54	2	8	20	39	0.7	4	12	30
	2($\phi = 35°$)	2	9	23	45	2	6	15	31	0.4	3	8	21
D	1($\phi = 30°$)	9	21	37	57	6	13	25	40	2	6	14	27
	2($\phi = 35°$)	7	17	32	51	4	11	20	35	1	4	10	22
	3($\phi = 40°$)	5	14	28	46	3	9	17	30	0.5	3	7	16

After an earthquake event the functionality of the bridge is important for evacuation, emergency and rescuing purposes. The fragility functions provide a means of quantifying this functionality of bridges in terms of their probability of exceedance of a particular damage state for given PGA. Table 5.3 shows the probability of exceedance of different damage states of a bridge abutment situated in different seismic zones defined in IS 1893 (2016).

The following observations can be made from the probability table of different damage states for different seismic zones:

1. The foundation shows a significant influence on the damage probability for all the damage states in lower seismic zones (I, II) for the same backfill.
2. For a given backfill soil, there is no significant influence of foundation type on the probability of all the three damage states for higher seismic zones (IV, V).
3. The probability of damage decreases for all damage states for both the foundation soil type (Type C and D), with increase in backfill friction angle, ϕ, density, γ, and shear wave velocity, V_s.
4. The change in probability of damage, with change in backfill is more pronounced in case of foundation soil Type C than in case of foundation soil Type D.

5.8 Summary

An extensive numerical simulation using 2D non-linear model with over 600 Incremental Dynamic Analysis (IDA) is performed in order to estimate the response of an abutment-backfill system in a seismic event. An attempt has been made to expand the existing framework of development of fragility functions for abutments with inclusion of soil non-linearity. The change in system's response is studied with variation in the properties of retained backfill and supporting foundation soil. The response of the system is studied in terms of the residual displacement of the top of abutment with respect to the free field condition. This residual displacement, $U_{h,\ Residual}$, is then used in the damage state definitions to develop fragility curves. The distribution of the shear forces and bending moment envelop in a seismic event has also been discussed.

The response of the system with increase in soil friction angle, ϕ, and density, γ, has been found to decrease for backfill resting on both foundation Type C and D. A wide range of variation is observed in the response corresponding to different ground motions. This may be attributed to the fact that there is a wide range of forcing frequency of ground motions and the system responds strongly to ground motions with forcing frequency close to the natural frequency of the system. Moreover, the backfill resting on foundation Type C have been found to reach the limit of a particular damage state earlier than those resting

on foundation Type D. A possible reason might be presence of natural frequency of the foundation system Type C closer to the forcing frequency of the ground motions selected.\

The influence of variation in backfill soil properties is observed more in higher damage states (collapse state DS_3). There is no significant change in the lower damage states (DS_1, DS_2) with change in backfill friction angle and shear strength parameters. The distribution of bending moment and shear force envelop along the height show more or less a uniformly distributed (UDL) or uniformly varying load (UVL) distribution in case of a seismic event behind the backfill.

The large variation in the response is partially due to the discrepancy in selection of ground motion. A further study can be performed for the ground motion selection procedure in case of soil-structure coupled system.

Chapter 6 Conclusions and Scope for future work

6.1 Conclusions

The primary objective of this dissertation work was to understand the seismic behavior of coupled abutment-backfill system and assess their seismic fragility. Initially, the behavior of the system is studied with pseudo-static methodology for a simple problem of a vertical wall retaining a horizontal backfill. The influence of backfill soil friction angle, wall-backfill interface angle and horizontal seismic coefficient on the pressure coefficients and pressure distribution along the height of wall has been explored. In continuation, the response of the coupled abutment-foundation-backfill system in terms of residual horizontal displacement during a seismic event has been studied with increase in ground motion intensity (in terms of PGA). The results of the Incremental Dynamic Analysis (IDA) are than used to develop seismic fragility curves. The specific conclusions of the study are presented in the following sections.

6.1.1 Estimation of Seismic Earth Pressure using Pseudo-Static Methodology

1. It has been observed that passive seismic earth pressure coefficient, K_p^+ corresponding to wall movement opposite to the direction of acceleration, gradually increases and passive seismic earth pressure coefficient, K_p^- corresponding to wall movement in the direction of acceleration, gradually decreases with the increase in horizontal seismic coefficient.
2. It has also been observed that active earth pressure coefficients, K_a^+ for wall movement in the direction of acceleration, gradually increases and active earth pressure coefficients, K_a^-, for wall movement in the opposite direction of acceleration, gradually decreases with the increase in horizontal seismic coefficient.
3. It has been found that with increase in soil friction angle, ϕ, or with increase in backfill-wall interface angle, δ, both passive pressure coefficients (K_p^+, K_p^-) increase.
4. It has also been found that with increase in soil friction angle, ϕ, or with increase in backfill-wall interface angle, δ, both active pressure coefficients (K_a^+, K_a^-) decrease.
5. In presence of gravity loading only, the active pressure envelop is distributed in triangular pattern along the height of wall. Whereas, in presence of gravity and

seismic loading (as horizontal seismic coefficient), the active and passive pressure envelops are distributed in trapezoidal shape along the height of wall.

6.1.2 Fragility Analysis

5. The bending moment at the base of the abutment is much higher than the case of retaining wall. This is due to the participation of dead load of the superstructure in a seismic event.
6. The peak ground acceleration to cause minor damage (DS_1 - 0.12 m), moderate damage (DS_2 - 0.3 m) and collapse damage (DS_1 - 0.48 m) increases for both the foundations (Type C and D), with increase in backfill friction angle, ϕ, and density, γ.
7. The response of the abutment also depends on the foundation underneath. It is interesting to note that although shear modulus, cohesion, density, friction angle and other soil parameters are higher for Foundation Soil Type C than Type D, abutment reaches collapse state at a smaller PGA for foundation Type C than Type D. The possibility of natural frequency of Type C close to forcing frequency of the ground motions might be a reason in amplification of its response.
8. A large variation in the systems' response can be observed corresponding to different ground motions. This variation is attributed to a wide range of forcing frequencies of the ground motions.
9. A weaving nature is observed in the dynamic capacity curve with increasing PGA values for some ground motions. This may be due to change in the frequency of the ground motion at the level of the abutment foundation due to nonlinearity of foundation soil and change in the frequency of vibration of abutment itself due to nonlinearity of the backfill material.

6.2 Recommendations for Future Work

The research work presented in this dissertation can be further extended by conducting the following studies:

1. The influence of soil dilatancy needs to be studied on the earth pressure coefficient and its distribution along the height of the wall.

2. The present study considers dry homogenous soil as backfill material, which may not represent the actual field situation. Additional research work considering material heterogeneity, is recommended.
3. The present study is based on 2D FE simulation of the abutment-backfill system. An extension using 3D simulations is recommended.
4. The seismic fragility curves presented in this dissertation are for abutment resting on flat ground. Future works towards developing fragility curves for abutments should incorporate effect of slope.
5. In the present study soil is modelled with a curvilinear elastic perfectly plastic shear stress-strain curve. Use of an advance nonlinear soil model is recommended to account for the complete stress-strain curve.
6. The abutment is modelled to remain elastic in studying the abutment-backfill system response during a seismic event. The influence of abutment material nonlinearity should also be explored in the future works.

References

1. “ABAQUS.” (2016). ABAQUS Documentation, Dassault Systèmes, Providence, RI, USA.
2. Anoosh, S., Rollins, K. M., and Mike, K. (2007). “Nonlinear Soil–Abutment–Bridge Structure Interaction for Seismic Performance-Based Design.” *Journal of Geotechnical and Geoenvironmental Engineering*, American Society of Civil Engineers, 133(6), 707–720.
3. Argyroudis, S., and Kaynia, A. M. (2015). “Analytical seismic fragility functions for highway and railway embankments and cuts.” *Earthquake Engineering & Structural Dynamics*, Wiley Online Library, 44(11), 1863–1879.
4. Argyroudis, S., Kaynia, A. M., and Pitilakis, K. (2013). “Development of fragility functions for geotechnical constructions: application to cantilever retaining walls.” *Soil Dynamics and Earthquake Engineering*, Elsevier, 50, 106–116.
5. Argyroudis, S., Palaiochorinou, A., Mitoulis, S., and Pitilakis, D. (2016). “Use of rubberised backfills for improving the seismic response of integral abutment bridges.” *Bulletin of Earthquake Engineering*, 14(12), 3573–3590.
6. ASCE/SEI 41-17 (2017). "Seismic Evaluation and Retrofit of Existing Buildings." American Society of Civil Engineers, Reston, Virginia.
7. Al Atik, L., and Sitar, N. (2010). “Seismic earth pressures on cantilever retaining structures.” *Journal of geotechnical and geoenvironmental engineering*, American Society of Civil Engineers, 136(10), 1324–1333.
8. Baris Darendeli, M. (2001). “Development of New Family of Normalized Modulus Reduction and Material Damping Curves.”
9. Beygi, M., Vali, R., Porhoseini, R., Keshavarz, A., and Maleksaeedi, E. (2018). “The effect of rotational stiffness on the behaviour of retaining wall.” *International Journal of Geotechnical Engineering*, Taylor & Francis, 1–12.
10. Bowels, J. E. (1996). *Foundation Analysis and Design*. (J. E. Bowles, ed.), McGraw-Hill Companies, Inc., Singapore.
11. Brando, M. (2012). “Seismic performance of bridges during Canterbury earthquakes.” Italy.
12. Caltabiano, S., Cascone, E., and Maugeri, M. (2000). “Seismic stability of retaining walls with surcharge.” *Soil Dynamics and Earthquake Engineering*, Elsevier, 20(5–8), 469–476.

13. Caltabiano, S., Cascone, E., and Maugeri, M. (2012). “Static and seismic limit equilibrium analysis of sliding retaining walls under different surcharge conditions.” *Soil Dynamics and Earthquake Engineering*, Elsevier, 37, 38–55.
14. Chouw, N., and Hao, H. (2005). “Study of SSI and non-uniform ground motion effect on pounding between bridge girders.” *Soil Dynamics and Earthquake Engineering*, Elsevier, 25(7–10), 717–728.
15. El-Emam, M. M., Bathurst, R. J., and Hatami, K. (2004). “Numerical modeling of reinforced soil retaining walls subjected to base acceleration.” *13th World Conference on Earthquake Engineering*.
16. Ettema, R., Ng, K., Chakradhar, R., Fuller, J., and Kempema, E. W. (2015). “Failure of spill-through bridge abutments during scour: Flume and field observations.” *Journal of Hydraulic Engineering*, American Society of Civil Engineers, 141(5).
17. Garini, E., Tsantilas, L., and Gazetas, G. (2016). “Seismic Response of Cantilever Retaining Walls: Verification of Centrifuge Experiments.” *1st International Conference on Natural Hazards & Infrastructure*, Chania, Greece.
18. Gharavi, A., and Bargi, K. (2012). “Seismic Analysis of L-shaped Quay Walls Considering Soil-Structure Interaction.” *15th World Conference on Earthquake Engineering*, Lisbon.
19. Huang, C.-C., Wu, S.-H., and Wu, H.-J. (2009). “Seismic Displacement Criterion for Soil Retaining Walls Based on Soil Strength Mobilization.” *Journal of Geotechnical and Geoenvironmental Engineering*, American Society of Civil Engineers, 135(1), 74–83.
20. IS1893 (2016). "Criteria for Earthquake Resistance Design of Structures, Part 1 Genera Provisosns and Buildings", Bureau of Indian Standards,New Delhi.
21. Jianfeng, Z., Andrus, R. D., and Hsein, J. C. (2005). “Normalized Shear Modulus and Material Damping Ratio Relationships.” *Journal of Geotechnical and Geoenvironmental Engineering*, American Society of Civil Engineers, 131(4), 453–464.
22. Khatri, V. (2019). “Determination of passive earth pressure with lower bound finite elements limit analysis and modified pseudo-dynamic method.” *Geomechanics and Geoengineering*, 1–12.
23. Krabbenhoft, K. (2018). “Static and seismic earth pressure coefficients for vertical walls with horizontal backfill.” *Soil Dynamics and Earthquake Engineering*, Elsevier, 104, 403–407.

24. Kuhlemeyer, R. L., and Lysmer, J. (1973). “Finite element method accuracy for wave propagation problems.” *Journal of Soil Mechanics and Foundation Division*, 421–427.
25. Kumar, J. (2001). “Seismic passive earth pressure coefficients for sands.” *Canadian Geotechnical Journal*, NRC Research Press, 38(4), 876–881.
26. Lee, C., Kang, Y. J., and Lee, H. Y. (2004). “A method for nonlinear dynamic response analysis of semi-infinite foundation using mapping.” *Transactions of the Japan Society for Computational Engineering and Science*, 11(2), 93–99.
27. Loukidis, D., Chakraborty, T., and Salgado, R. (2008). “Bearing capacity of strip footings on purely frictional soil under eccentric and inclined loads.” *Canadian Geotechnical Journal*, NRC Research Press, 45(6), 768–787.
28. M. Duncan, J., and Chang, C. Y. (1970). “Nonlinear analysis of stress and strain in soils.” *Proceedings Paper: Journal of Soil Mechanics and Found Division ASCE*, 96, 1629–1653.
29. Modha, K. G. (2018). “Spectral Amplification of Ground Motion due to Triangular hill features.” M.Tech. Thesis, Department of Earthquake Engineering, Indian Institute of Technology Roorkee.
30. Morrison Jr., E. E., and Ebeling, R. M. (1995). “Limit equilibrium computation of dynamic passive earth pressure.” *Canadian Geotechnical Journal*, NRC Research Press, 32(3), 481–487.
31. Musharraf-uz, Z. M., Desai, C. S., and Drumm, E. C. (1984). “Interface Model for Dynamic Soil-Structure Interaction.” *Journal of Geotechnical Engineering*, American Society of Civil Engineers, 110(9), 1257–1273.
32. Mylonakis, G., Kloukinas, P., and Papantonopoulos, C. (2007). “An alternative to the Mononobe–Okabe equations for seismic earth pressures.” *Soil Dynamics and Earthquake Engineering*, Elsevier, 27(10), 957–969.
33. Olmos, B. A., and Roesset, J. M. (2008). “Soil structure interaction effects on base isolated bridges.” *14th World Conf. On Earthquake Engineering, China*.
34. Pain, A., Choudhury, D., and Bhattacharyya, S. K. (2015). “Seismic stability of retaining wall–soil sliding interaction using modified pseudo-dynamic method.” *Géotechnique Letters*, Thomas Telford Ltd, 5(1), 56–61.
35. Pitilakis, K., Crowley, H., and Kaynia, A. M. (2014a). “SYNER-G: typology definition and fragility functions for physical elements at seismic risk.” *Geotechnical, Geological and Earthquake Engineering*, Springer.

36. Psarropoulos, P. N., Klonaris, G., and Gazetas, G. (2005). “Seismic earth pressures on rigid and flexible retaining walls.” *Soil Dynamics and Earthquake Engineering*, Elsevier, 25(7–10), 795–809.
37. Purkar, M. S., and Kute, S. (2015). “Finite element analysis of a concrete-rigid wall retaining a reinforced backfill.” *International Journal of Geo-Engineering*, Springer, 6(1), 14.
38. Raj, D. (2018). “Seismic Behaviour of Foundations and Buildings on Slopes.” Ph.D. Thesis, Department of Earthquake Engineering, Indian Institute of Technology Roorkee.
39. Rajesh, B. G., and Choudhury, D. (2017). “Seismic passive earth resistance in submerged soils using modified pseudo-dynamic method with curved rupture surface.” *Marine Georesources & Geotechnology*, Taylor & Francis, 35(7), 930–938.
40. Senthil, K., Iqbal, M. A., and Kumar, A. (2014). “Behavior of cantilever and counterfort retaining walls subjected to lateral earth pressure.” *International Journal of Geotechnical Engineering*, Taylor & Francis, 8(2), 167–181.
41. Sextos, A. G., Manolis, G. D., Athanasiou, A., and Ioannidis, N. (2017). “Seismically induced uplift effects on nuclear power plants. Part 1: Containment building rocking spectra.” *Nuclear Engineering and Design*, North-Holland, 318, 276–287.
42. Shamsabadi, A., Xu, S.-Y., and Taciroglu, E. (2013). “A generalized log-spiral-Rankine limit equilibrium model for seismic earth pressure analysis.” *Soil Dynamics and Earthquake Engineering*, 49, 197–209.
43. Shiau, J. I. M. S., Augarde, C. E., Lyamin, A. V, and Sloan, S. W. (2008). “Finite Element Limit Analysis of Passive Earth Resistance in Cohesionless soils.” *Soils and foundations*, 48(6), 843–850.
44. Shukla, S. K. (2010). “Closure to ‘Active Earth Pressure on Retaining Wall for c-ϕ Soil Backfill under Seismic Loading Condition’ by SK Shukla, SK Gupta, and N. Sivakugan.” *Journal of Geotechnical and Geoenvironmental Engineering*, American Society of Civil Engineers, 136(11), 1585.
45. Sotiris, A., Stergios, M., Kaynia, A. M., and Winter, M. G. (2019). “Fragility Assessment of Transportation Infrastructure Systems Subjected to Earthquakes.” *Geotechnical Earthquake Engineering and Soil Dynamics V*, Proceedings, 174–183.
46. Soubra, A.-H. (2000). “Static and seismic passive earth pressure coefficients on rigid retaining structures.” *Canadian Geotechnical Journal*, NRC Research Press, 37(2), 463–478.

47. Subba Rao, K. S., and Choudhury, D. (2005). “Seismic Passive Earth Pressures in Soils.” *Journal of Geotechnical and Geoenvironmental Engineering*, American Society of Civil Engineers, 131(1), 131–135.
48. Tiznado, J. C., and Rodriguez-Roa, F. (2011). “Seismic lateral movement prediction for gravity retaining walls on granular soils.” *Soil Dynamics and Earthquake Engineering*, Elsevier, 31(3), 391–400.
49. Tokimatsu, K., Suzuki, H., and Sato, M. (2005). “Effects of inertial and kinematic interaction on seismic behavior of pile with embedded foundation.” *Soil Dynamics and Earthquake Engineering*, Elsevier, 25(7–10), 753–762.
50. Xu, S.-Y., Kannangara, K. K. P. M., and Taciroglu, E. (2018). “Analysis of the stress distribution across a retaining wall backfill.” *Computers and Geotechnics*, 103, 13–25.
51. Yingwei, W., and Shamsher, P. (2019). “On Seismic Displacements of Rigid Retaining Walls.” *Analysis and Design of Retaining Structures against Earthquakes*, Proceedings.
52. Zamiran, S., and Osouli, A. (2018a). “Seismic motion response and fragility analyses of cantilever retaining walls with cohesive backfill.” *Soils and Foundations*, Elsevier, 58(2), 412–426.
53. Zamiran, S., and Osouli, A. (2018b). “Fragility Analysis of Seismic Response of Cantilever Retaining Walls with Cohesive and Cohesionless Backfill Materials.” *The International Association of Foundation Drilling*, Orlando, Florida.
54. Zhu, Y. L., Yu, J., Zhou, J. F., Tu, B. X., and Cai, Y. Y. (2018). “Calculation of earth pressure on rigid retaining walls with considerations to the seismic load and soil stress-deflection.” *Journal of Vibroengineering*, 20(3).